Asian Journal of Pharmaceutical Sciences 15 (2020) 759–776

Available online at www.sciencedirect.com

ScienceDirect

journal homepage: www.elsevier.com/locate/AJPS

Original Research Paper

# Enhanced lysosome escape mediated by 1,2-dicarboxylic-cyclohexene anhydride-modified poly-L-lysine dendrimer as a gene delivery system

*Jianmin Shen*[a,b,1,*], *Jing Chen*[a,b,1], *Jingbo Ma*[a,b], *Linlan Fan*[c], *Xiaoli Zhang*[b], *Ting Yue*[a,b], *Yaping Yan*[a], *Yuhang Zhang*[a]

[a] *School of Life Sciences, Lanzhou University, Lanzhou 730000, China*
[b] *Shenzhen Following Precision Medical Research Institute, Shenzhen 518001, China*
[c] *School of Basic Medical Sciences, Lanzhou University, Lanzhou 730000, China*

ARTICLE INFO

*Article history:*
Received 3 July 2019
Revised 7 October 2019
Accepted 10 December 2019
Available online 6 February 2020

*Keywords:*
Antisense oligodeoxynucleotide (ASODN)
Gene delivery
Dendrigraft poly-L-lysines (DGL)
Lysosomal escape
Tumor targeting

ABSTRACT

Antisense oligodeoxynucleotide (ASODN) can directly interfere a series of biological events of the target RNA derived from tumor cells through Watson-Crick base pairing, in turn, plays antitumor therapeutic roles. In the study, a novel HIF-1$\alpha$ ASODN-loaded nanocomposite was formulated to efficiently deliver gene to the target RNA. The physicochemical properties of nanocomposite were characterized using TEM, FTIR, DLS and zeta potentials. The mean diameter of resulting GEL-DGL-FA-ASODN-DCA nanocomposite was about 170–192 nm, and according to the agarose gel retardation assay, the loading amount of ASODN accounted for 166.7 mg/g. The results of cellular uptake showed that the nanocomposite could specifically target to HepG2 and Hela cells. The cytotoxicity assay demonstrated that the toxicity of vectors was greatly reduced by using DCA to reversibly block the cationic DGL. The subcellular distribution images clearly displayed the lysosomal escape ability of the DCA-modified nanocomposite. *In vitro* exploration of molecular mechanism indicated that the nanocomposite could inhibit mRNA expression and *HIF-1α* protein translation at different levels. *In vivo* optical images and quantitative assay testified that the formulation accumulated preferentially in the tumor tissue. *In vivo* antitumor efficacy research confirmed that this nanocomposite had significant antitumor activity and the tumor inhibitory rate was 77.99%. These results manifested that the GEL-DGL-FA-ASODN-DCA nanocomposite was promising in gene therapeutics for antitumor by interacting directly with target RNA.



* Corresponding author. School of Life Sciences, Lanzhou University, No. 222 Tianshui South Road, Lanzhou 730000, China. Tel.: +86 15117266908
*E-mail address:* shenjianmin@lzu.edu.cn (J.M. Shen).
[1] Co-first author
Peer review under responsibility of Shenyang Pharmaceutical University.

https://doi.org/10.1016/j.ajps.2019.12.001

## 1. Introduction

Cancer has been a serious threat to human health worldwide [1], and conventional therapeutic means such as surgery, chemotherapy and radiotherapy are not ideal due to toxicity and side effect, drug resistant and inadequate treatment [2,3]. Therefore, new anticancer strategies are urgently required. Cancer is a kind of genetic disease [4]. Gene therapy, such as antisense therapeutics, is a promising therapeutic method for cancer treatment [5]. Local hypoxia caused by immoderate and rapid proliferation of cancer cells is an important feature of solid tumors [6]. Hypoxia inducible factor-1 (HIF-1) is a core transcription factor that regulates oxygen homeostasis, and plays a key role in tumor angiogenesis, energy metabolism, invasion and metastasis [7,8]. The availability of its subunit (HIF-1$\alpha$) determines its activity [9]. HIF-1$\alpha$ is involved in variety of tumor signaling pathways, regulating cell survival, inhibiting tumor cell apoptosis, and metabolic remodeling [10]. Therefore, HIF-1$\alpha$ serves as a potential molecular target for developing cancer therapeutics. Antisense oligodeoxynucleotide (ASODN)-based therapeutic strategies have aroused great concern in the last two decades, and ASODN-mediated intervention is a very hopeful therapeutic approach [5]. This therapeutic method involved the manipulation of target gene expression by competitively binding a HIF-1$\alpha$ ASODN sequence (5′-GCC GGC GCC CTC CAT-3′) to the segment of the target mRNA [11–13], which could lead to RNase-H-mediated cleavage of the target mRNA [14] or inhibition of transcription [15].

The HIF-1$\alpha$ ASODN fragment, however, is non-specific *in vivo*, and easy to cause toxicity and side effects [16]. And it can be degraded by nuclease from both tissues and cells [17], which leads to loss of therapeutic activity. Furthermore, the bare HIF-1$\alpha$ ASODN fragment also has poor intracellular delivery because the negatively charged ASODN can induce charge repulsion against the anionic cell surface [18,19]. In particular, it is thought to be an important obstacle for gene delivery *in vivo* that ASODN fragment is trapped in lysosomes and further degraded [3,20]. As a consequence, it is crucial for gene therapy to develop a gene delivery vector with excellent properties such as targeting specificity, cellular internalization, and highly efficient lysosomal escape ability.

Cationic polymers, such as polyethyleneimine (PEI) and polyamidoamine (PAMAM), are ideal gene delivery carriers because they have a low immune response and are easy to be assembled and decorated [21]. Especially, when transported to lysosomes, the dendritic macromolecules will absorb a large amount of protons in this acidic environment, which results in different transmembrane voltages inside and outside the cell membrane [22], in turn, the inflow of $H_2O$, $Cl^-$and $H^+$ in the cytoplasm to balance the acidic environment of lysosomes. Eventually the lysosome membrane swells and ruptures, releasing the cationic polymers and their cargos to the cytoplasm [23,24]. This is known as a proton sponge effect [22] which can mediate the escape of ASODN from the lysosomes and facilitates recombination with the target gene [25,26]. These cationic polymers, however, possess high cytotoxicity and poor biodegradability. So, their application is greatly blocked [27,28]. In contrast, dendrigraft poly-L-lysine (DGL) taking poly-L-lysine (PLL) as structural units [29] not only retains the main characters of PLL, but also has many excellent properties such as flexible architecture, biocompatibility, nontoxicity, and good transmembrane capacity [30]. Furthermore, DGL is completely biodegradable, and its degradation product lysine is essential amino acids of the human body, which reduces greatly the toxicity and side effects of the carriers [31]. In the current studies, DGL has been widely used as the delivery carriers of drugs (doxorubicin, paclitaxel and oxaliplatin) [32] and genes (DNA and RNA) [33]. It is worth mentioning that DGL has a large number of positive charges, which is beneficial to electrostatic attraction with the negatively charged ASODN to form a stable composite in the synthesis process [33,34]. This makes it possible to transport ASODN to target genes in cells, realizing the anti-cancer efficacy of genes.

Unfortunately, common DGL has just a few nanometers to a dozen nanometers in particle size [35] and is easily excreted and removed by the kidney [36], leading to the poor bioavailability of genes [37]. Besides, the highly positive charged DGL can induce the agglutination of blood components consisting of albumin and erythrocytes in the bloodstream by their strong non-specific electrostatic interactions [38]. This agglutination often causes embolism and inflammation [39], showing that DGL vectors can also induce toxicities. In addition, the amino groups of lysine from DGL have usually already been protonated at the physiological conditions (pH 7.4), and DGL cannot further absorb protons after it is transported to the cell lysosomes [40,41], which will weaken the proton sponge effect and limit the escape of the vector from lysosomes. Therefore, the research idea of this work was to optimize the particle size of vectors, and block reversibly the positive charges of DGL by modifying DGL, which was aimed at the long blood circulation time, low toxicity, and prominent proton sponge effect.

Gelatin (GEL) is a kind of natural polymer protein with good biocompatibility and degradability, and is widely used for synthetizing drug carrier [42]. GEL nanoparticles with ideal size (50–200 nm) can be prepared by optimizing various parameters. In the present study, the vector with size range of 150–190 nm was firstly synthetized by taking the GEL nanoparticles with desired diameter as the inner core and grafting DGL on its surface. The purpose of selecting this particle size range is to prolong blood circulation time and accumulate preferentially the vectors into solid tumors by the enhanced permeability and retention (EPR) effect [43]. On this basis, in order to enhance the specific targeting of vectors to tumor cells, DGL was further modified with ligand folate (FA) so that cell internalization was efficiently realized through FA receptor-mediated endocytosis because of the overexpress of FA receptors in many cancer cells [44,45].

In order to improve the ability of lysosomal escape, DGL has been chemically modified using various ligands. These moieties include adenovirus [46], chloroquine [47], and membrane-fusion peptide, such as melittin [48], N-terminal amphiphilic anionic peptide of influenza virus haemagglutinin (HA2) [49], and PAsp (DET) [50]. They can induce remarkable lysosomal lysis by means of membrane

fusion and proton sponge effect. However, these peptides or organic chemicals have more or less cytotoxicity [51,52]. By contrast, 1, 2-dicarboxylic-cyclohexene anhydride (DCA) is a small molecular acid anhydride [53,54], and has been used for modification of macromolecule in many studies [55,56]. Thus, DCA acted as another ligand to modify the amino groups on DGL in present study. The resultant DGL-DCA composite was very stable over 24 h at normal physiological fluids (pH 7.4). Furthermore, the carboxyl groups introduced from DCA made DGL carry the enough negative charges, which could avoid the aggregation of the blood components and reduce toxicity and side effects. What was more, when the vectors were transported into lysosomes, the $\beta$-amide bonds formed between DGL and DCA were apt to hydrolysis due to the susceptibility to the acidic environment, resulting in the exposure of primary $\varepsilon$-amino groups of DGL. DGL absorbed immediately a large amount of the protons in lysosomes, in turn, triggering a proton sponge effect, and finally achieving escape from lysosomes. Herein, DGL-DCA composite was used to exhibit a pH-triggered charge-reversible moiety. In conclusion, it will provide a certain reference for the gene therapy of tumors to develop a gene delivery system with excellent comprehensive performances, including a safety, specific targeting, cellular internalization and lysosomal escape capacity (Graphical Abstract).

## 2. Materials and methods

### 2.1. Materials

Dendrigraft poly-L-lysine (DGL-G5, MW = 172,300) was obtained from Colcom (Montpellier Cedex, France). 1-Ethyl-3-(3-dimethylaminopropyl) carbodiimide hydrochloride (EDAC), N-hydroxysuccinimide (NHS) and gelatin (type A) from porcine skin were purchased from Sigma-Aldrich (Shanghai, China). One dual functional polyethylene glycol (PEG) with one end of amine group protected by Fmoc and the other end of carboxyl group (Fmoc-$NH_2$-$PEG_{2000}$-COOH, MW = 2238), another dual functional PEG with one end of folate and the other end of carboxyl group (FA-$PEG_{2000}$-COOH, MW = 2487.4), and 1, 2-dicarboxylic-cyclohexene anhydride (DCA, purity 96%) were gotten from Xi'an Ruixi biological Technology Co. Ltd. (Xian, China). HIF-1$\alpha$ antisense phosphorothioate oligodeoxynucleotide (ASODN) and Cy5.5-labeled HIF-1$\alpha$ antisense phosphorothioate oligodeoxynucleotide (ASODN-Cy5.5) with an excitation wavelength of 675 nm and an emission wavelength of 695–710 nm were synthesized by Sangon Biotech Co. Ltd. (Shanghai, China) according to published sequences (antisense sequence: 5′-GCC GGC GCC CTC CAT-3′, MW: 4714, and Cy5.5-labeled antisense sequence: 5′-GCC GGC GCC CTC CAT-Cy5.5–3′, MW: 5488). Anhydrous cobalt dichloride ($CoCl_2$) was provided by Sun chemical technology Co. Ltd (Shanghai, China). Dulbecco's modified Eagle's medium (DMEM), RPMI 1640 medium, penicillin, streptomycin, ampicillin, trysin, and Lyso-Tracker-Green DND-26 were purchased from Themo Fisher Scientific (Waltham, MA, USA). 4, 6-Diamino-2-phenyl indole (DAPI) was provided by Vector laboratories (USA). Fetal bovine serum (FBS) was obtained from Biological Industries (Israel). 3-(4,5-Dimethylthiazd-2,5-diphenyl tetrazodium bromide (MTT) and phosphate buffer saline (PBS) and radio immunoprecipitation assay (RIPA) lysis buffer were provided by Solarbio Reagent Co. Ltd. (Beijing, China). Cy5.5-labeled N-hydroxysuccinimide (NHS) ester (Cy5.5-NHS with an excitation wavelength of 675 nm and an emission wavelength of 710 nm) was purchased from APExBIO (Houston, TX, USA). Human HIF-1$\alpha$ enzyme-linked immunoassay kit (HIF-1$\alpha$ ELISA Kit: E-EL-H1277c) was received from Elabscience (Wuhan, China).

Human hepatocytes cancer cells (HepG2), human cervical carcinoma cells (HeLa) and murine hepatocytes cancer cells (H22) were purchased from the cell bank of shanghai science academe (Shanghai, China). Male Balb/c mice (4-week old, $20 \pm 2$ g) were obtained from experiment animal center of Lanzhou University (Lanzhou, China). The mice were raised under standard feeding conditions. All animal experiments were followed the principle of the experiment animal administrate committee of Lanzhou University.

### 2.2. Preparation of step-by-step nanocomposites

#### 2.2.1. Preparation of DGL-$NH_2$ and DGL-$NH_2$-FA

In the first synthesis, Fmoc-$NH_2$-$PEG_{2000}$–COOH (10 mg, 0.0045 mmol) and EDAC (8.63 mg, 0.045 mmol) were dissolved in anhydrous dimethyl sulfoxide (1.5 ml). The mixture solution was shaken for 1.5 h at room temperature. Then, NHS (5.18 mg, 0.045 mmol) dissolved in 1 ml of anhydrous dimethyl sulfoxide was added, and the mixture was shaken for another 1.5 h at room temperature to activate the carboxyl groups of Fmoc-$NH_2$-$PEG_{2000}$–COOH. The resulting mixture solution was added dropwise to DGL (77.53 mg, 0.00045 mmol) dissolved in 2 ml buffer A (50 mM PBS containing 0.1 M NaCl, pH7.4) under shaking at room temperature. After shaken for another 24 h, the mixture was dialyzed against $dH_2O$ (500 ml × 9 times) through a membrane with a MWCO of 8000–14 400 Da to remove excess reagents such as Fmoc-$NH_2$-$PEG_{2000}$-COOH, EDAC and NHS, followed by lyophilization to obtain product DGL-PEG-$NH_2$-Fmoc (abbreviated as DGL-$NH_2$). The DGL-$NH_2$ was simultaneously prepared two copies. The composition of DGL-$NH_2$ was confirmed by FTIR spectrum measured by a spectrophotometer (NEXUS 670 FTIR; Nicolet, USA). In the second synthesis, one of the resultant DGL-$NH_2$ was again dissolved in 2 ml above buffer A in one 20 ml of flask, followed by ultrasound for 3 min and shaking for 3 h. Subsequently, the carboxyl groups of FA-$PEG_{2000}$-COOH (11.2 mg, 0.0045 mmol) were activated using above-mentioned procedures by reacting with EDAC and NHS. Then, the activated FA-$PEG_{2000}$-COOH was added dropwise to DGL-$NH_2$ solution, and the reaction continued for another 24 h under shaking at room temperature. The product was dialyzed, lyophilized, and further confirmed by FTIR as mentioned above. The product was denoted by FA-$PEG_{2000}$-DGL-PEG-$NH_2$-Fmoc (abbreviated as DGL-$NH_2$-FA).

#### 2.2.2. Preparation of DGL-$NH_2$-asodn and DGL-$NH_2$-Fa-asodn

The freeze-dried products DGL-$NH_2$ with various weight were dissolved in 1 ml buffer A to prepare a series of concentrations (1, 2, 4, 6, 8, 10, 12, 14 and 16 mg/ml), respectively. ASODN powder was dissolved in 0.80 ml of 1 × TE buffer (10 mmol/l Tris•HCl; 1 mmol/l EDTA, pH 8.0) to reach a final concentration

of 0.47 mg/ml. The ASODN solutions were prepared nine copies and were added to a series of above DGL-$NH_2$ solution, respectively. Then, the mixtures were immediately vortexed for 30 s and incubated for another 4 h at room temperature. The products were denoted by DGL-$NH_2$-ASODN. Agarose gel electrophoresis was carried out to evaluate the binding ability of ASODN with DGL-$NH_2$, so that an optimum ratio between DGL-$NH_2$ and ASODN was confirmed. Subsequently, DGL-$NH_2$-FA-ASODN composites were also prepared by this method according to the optimum ratio explored. The binding ability of ASODN with DGL-$NH_2$-FA was also assessed. In order to subsequent imaging analysis *in vitro* and *in vivo*, Cy5.5-labled composites (DGL-$NH_2$-ASODN-Cy5.5, and DGL-$NH_2$-FA-ASODN-Cy5.5) were also prepared by replacing ASODN with ASODN-Cy5.5.

#### 2.2.3. *Preparation of DGL-$NH_2$-ASODN-DCA and DGL-$NH_2$-FA-ASODN-DCA*

Two copies of DCA (each one 197.8 mg) were dissolved in 4 ml DMSO, respectively. And DCA solutions were gradually mixed with above DGL-$NH_2$-ASODN and DGL-$NH_2$-FA-ASODN, respectively. pH was adjusted to 8.5 by adding NaOH solution during the reaction. The mixtures were shaken for 24 h. The solutions were dialyzed against $dH_2O$ (molecular weight cut off: 2000 Da) at pH 8.5 to remove free DCA. The products DGL-$NH_2$-ASODN-DCA and DGL-$NH_2$-FA-ASODN-DCA were obtained.

#### 2.2.4. *Preparation of GEL-DGL-FA-ASODN-DCA, GEL-DGL-FA-ASDON and GEL-DGL-ASDON-DCA*

In the first place, gelatin nanoparticles were synthesized by a two-step desolvation method [57]. First step, gelatin A (0.75 g) was dissolved in 15 ml of deionized water by heating to 40 °C. Heating was immediately stopped after gelatin dissolution, and 15 ml of acetone was added to the solution at a speed of 6.0 ml/min while stirring at 300 rpm. One minute later, the white colored supernatant was removed. Second step, the sediment was redissolved in deionized water (38.57 ml) at 40 °C. Half of the solution was removed, and the remaining half was adjusted to pH 2.8 using 1 M HCl. Acetone (48 ml) was added at a speed of 1.0 ml/min, while the mixture was continuously stirred at 600 rpm and 40 °C. Then, 1.48 ml of glutaraldehyde solution (25% glutaraldehyde: acetone = 7:30, v/v) was mixed with above gelatin solution at a rate of 50 μl/min for crosslinking reaction. The mixture was continuously stirred at 40 °C and 600 rpm for 7.5 h. When the acetone was evaporated to a final volume of 18 ml, the mixture was filtered through a membrane of 0.2 μm. And 0.24 ml of glycine solution (1 M) was added to stop reaction. The nanoparticles were separated from the mixture by centrifugation at 12 000 rpm for 30 min, washed three times using distilled water, then resuspended in 15 ml of distilled water for next use.

In the second place, GEL-DGL-FA-ASODN-DCA, GEL-DGL-FA-ASDON and GEL-DGL-ASDON-DCA nanocomposites were synthesized. Firstly, the carboxyl groups of three copies of above GEL suspension liquids (each one 813 μl) were activated by adding EDAC (0.43 mg) and NHS (0.26 mg) according to the method in the Section 2.2.1, respectively. The activated GEL was mixed dropwise with of above DGL-$NH_2$-FA-ASODN-DCA, DGL-$NH_2$-FA-ASODN and DGL-$NH_2$-ASODN-DCA solutions after the Fmoc moieties protecting the amino groups were removed by dimethylamine, and the mixtures were shaken for 24 h at room temperature. The mixtures were dialyzed against $dH_2O$ (500 ml × 9 times) through a membrane with a MWCO of 2000 Da and then lyophilized to obtain the final products GEL-DGL-FA-ASODN-DCA, GEL-DGL-FA-ASDON and GEL-DGL-ASODN-DCA. In addition, the solutions containing the final products in the dialysis bag were used for electrophoresis detection to evaluate whether the grafting GEL affected the stability of ASODN on nanocomposites.

### 2.3. *Characterization*

The morphologies of DGL-FA-ASODN-DCA, GEL and GEL-DGL-FA-ASODN-DCA nanoparticles were characterized by transmission electron microscopy (TEM, TecnaiG2 F30; FEI, USA) with an accelerating voltage of 200 kV. The particle sizes of DGL-FA-ASODN-DCA, GEL and GEL-DGL-FA-ASODN-DCA nanocomposites were measured using the BI-200SM dynamic light scattering (Brookerhaven; UK). The compositions of DGL, DGL-$NH_2$ and DGL-$NH_2$-FA were analyzed by FTIR spectrum measured by a spectrophotometer (NEXUS 670 FT-IR; Nicolet, USA). The zeta potentials of the DGL-FA-ASODN-DCA and GEL-DGL-FA-ASODN-DCA nanocomposites were measured by dynamic light scattering (DLS) analyzer (Malvern Zetasizer Nano 3600; UK) at pH 7.4, 6.8 and 5.0 at different time points after suspension (0, 1, 1.5, 2, 6, 10 and 24 h).

### 2.4. *Agarose gel retardation assay*

Agarose gel retardation assay was used to confirm the optimum ratio of precursors (DGL-$NH_2$ and ASODN), to determine the binding ability of DGL-$NH_2$-FA with ASODN, and to detect whether the subsequent modification on composites by DCA and GEL changed the stability of ASODN already uploaded. The resulting DGL-$NH_2$-ASODN, DGL-$NH_2$-FA-ASODN, DGL-$NH_2$-FA-ASODN-DCA and GEL-DGL-FA-ASODN-DCA nanocomposites were mixed with 4 μl 6 × loading buffer [30 mM EDTA, glycerol (36%, v/v), xylene cyanol FF (0.05%, w/v), bromophenol blue (0.05%, w/v)], and then electrophoresed on 1.5% (w/v) agarose gel containing ethidium bromide (0.25 g/ml of the gel), respectively. The same amount of free ASODN (2 μg/lane) and DGL-$NH_2$ (2 μg/lane) were used as controls. The gel was run for 20 min at 100 V in Tris-acetate running buffer (40 mM Tris-acetate, 1 mM EDTA, pH 8.3). ASODN motion retardation was observed by E-Gel Imager System (E-Gel Imager, Invitrogen, USA).

### 2.5. *Cellular uptake measurements*

The cellular uptake of the ASODN–Cy5.5-loaded nanocomposites was analyzed by flow cytometry. HepG2 and HeLa cells were seeded in six-well plates at a density of $4.5 \times 10^5$ cells /well and allowed to grow for 24 h, respectively. Subsequently, the cells were incubated with the different nanocomposites with an ASODN-Cy5.5 concentration of 5 μg/ml which were prepared using RPMI Medium 1640

(serum free and folic acid free). At different incubation time (1 h and 6 h), the solution was removed. The cells were washed three times with 1 ml of cold PBS (pH 7.4). Thereafter, the cells in each well were detached by adding 300 μl of trypsin. The mixtures were centrifuged at 4000 rpm at 4 °C for 5 min. The harvested cell precipitates were rinsed three times with above cold PBS to remove free fluorescence in the medium, followed by centrifugation again. Finally, the cell precipitates were resuspended in 600 μl of PBS for next analysis. Each sample was quickly analyzed on a flow cytometer (BDLSRFortessa, USA) for intracellular fluorescence detection by counting 10 000 events using the 675 nm for excitation and the 710 nm for emission. The untreated HepG2 and HeLa cells were used as control, respectively.

### 2.6. Subcellular distribution

The subcellular distribution of variation with time was monitored using a confocal laser scanning microscopy (CLSM, Olympus, FV-300, IX71) to verify the lysosomal escape of nanocomposites. The HepG2 cells were seeded in a 6-well plate ($2.5 \times 10^5$ cells/well) containing a glass cover slip at bottom in folate-deficient RPMI 1640 medium for 24 h. Then, the cells were incubated with GEL-DGL-FA-ASODN-Cy5.5-DCA, GEL-DGL-FA-ASODN-Cy5.5, GEL-DGL-ASODN-Cy5.5-DCA, DGL-FA-ASODN-Cy5.5-DCA, and free ASODN-Cy5.5 nanocomposites with an ASODN-Cy5.5 concentration of 30 μg/ml, respectively. At different indicated time (1, 2, 4 and 6 h), the solutions were removed, and the cells were washed 5 times with 1 ml of pre-warmed PBS to remove free dead cells and unbound ASODN or nanocomposites. The cells were further incubated with pre-warmed LysoTracker Green DND-26 probe for another 1 h to stain late endosomes/lysosomes. After the treatment, the cells were washed 5 times with pre-warmed PBS and fixed in 1 ml 4% paraformaldehyde for 15 min at room temperature. Finally, the nucleus was stained with DAPI for 15 min. The cells were washed and observed by CLSM with an excitation wavelength of 358 nm for DAPI (nucleus), 504 nm for late endosomes/lysosomes and 675 nm for ASODN-Cy5.5.

### 2.7. In vitro cytotoxicity

MTT assay was employed to measure the cytotoxicity of free ASODN and different nanocomposites at various concentrations on HepG2 and HeLa cells. The specific process was as follows: HepG2 and HeLa cells were seeded in 96-well plates (8000 cells/well) in 100 μl RPMI medium 1640 (folate free and serum free), respectively. After the cells were incubated for 24 h, the culture media were replaced with 100 μl fresh above medium containing 200 μM $CoCl_2$, and then the cells were further incubated for 4 h to establish a hypoxia model. After 4 h, the original medium was removed and replaced with new solutions containing free ASODN or nanocomposites with different ASODN concentrations (0.783, 1.563, 3.125, 6.25, 12.5, 25, 50 and 100 μg/ml), and the cells were incubated for another 24 h. Then, 10 μl of MTT was added to each well, and the cells were further incubated for 4 h. Finally, 150 μl of DMSO was used to dissolve the formazan crystals generated by live cells in each well. The cells without treatment were used as a control. Absorbance was measured at 490 nm using a microplate spectrophotometer (iMark$^{TM}$; Bio-Rad Laboratories Inc., Hercules, CA, USA). Each concentration is repeated six times. The cell viability was expressed as the percentage of the absorbance relative to the control cell group. Each experiment was repeated in triplicate.

### 2.8. HIF-1α mRNA level analysis

The HepG2 cells were seeded in a 6-well plate ($4.5 \times 10^5$ cells/well) in folate-deficient and serum-deficient RPMI 1640 medium for 24 h. Then, the hypoxia cells were induced by adding $CoCl_2$ as described in the Section 2.7. And the cells were treated with the different nanocomposites with an ASODN concentration of 0.8 μg/ml for 12 h. The total RNA from harvested cells was extracted according to the manufacturer's instructions of TransZol Up Plus RNA Kit (Beijing TransGen Biotech Co., Ltd.; Beijing, China). And 1000 ng of total RNA was reversely transcribed using Power RT Kit and Oligo dT or Random Primer (50 μM) (Bioteke Corporation, Beijing, China). The cDNA from the first-strand synthesis was diluted 10 times with $ddH_2O$. Quantitative real-time PCR (qRT-PCR) was performed by mixing the cDNA diluent (2 μl), 2 × Premix (10 μl, Power 2 × SYBR Real-time PCR Premixture, Bioteke Corporation, Beijing, China), forward primers (0.4 μl), reverse primers (0.4 μl) and sterile $H_2O$ (7.2 μl) to a final volume of 20 μl. The following primer pairs were used: HIF-1α forward 5′-TACTAAAGGACAAGTCACCACA-3′ and reverse 5′-CTGAATAATACCACTCACAACG-3′, β-actin forward 5′-TGGCATCCACGAAACTACC-3′ and reverse 5′-ATCTCCTTCTGCATCCTGTC-3′. The PCR procedure was 50 °C for 2 min and 95 °C for 10 min. Then 40 cycles were carried out at 95 °C for 15 s and 60 °C for 1 min. Relative quantities of target mRNA sequence were calculated from the set threshold cycle using the iCycler iQ Real-time Detection System software. All reactions were repeated in triplicate.

### 2.9. Enzyme-linked immunosorbent assay (ELISA)

The hypoxia HepG2 cells was induced and treated with different ASODN-loaded nanocomposites as described in the Section 2.8. Total protein was extracted from the cells with RIPA lysis buffer (Beijing Solarbio Science & Technology Co., Ltd.; Beijing, China) in an ice bath. Total protein concentration was measured using an Enhanced BCA Protein Assay Kit (Beyotime biotechnology, China). The level of HIF-1α protein contained in the total protein was assessed using the Human HIF-1α ELISA Kit (Elabscience: E-EL-H1277c). The HIF-1α protein content was calculated according to the standard curve. Results were expressed as pg/μg protein.

### 2.10. Establishment of H22 tumor-bearing animal models

Male Balb/c mice (BW: 20 ± 2 g) were acclimatized at 22 ± 1 °C and 50%–60% relative humidity under natural light/dark conditions. All animal experiments were in accordance with the guidelines approved by the Ethics Committee of Lanzhou University. Each mouse was received subcutaneous inoculation of $2 \times 10^6$ H22 cells at the right front oxter of mouse. Tumor-bearing mice were used for

the following tests *in vivo* when tumor volume reached 50 $mm^3$.

### 2.11. *In vivo imaging analysis*

Eighteen H22 tumor-bearing mice were randomly divided into six groups ($n = 3$ per group). Each mouse from control group (group a) was injected 0.2 ml of saline solution. And 0.2 ml of ASODN-Cy5.5 (group b), DGL-ASODN-Cy5.5 (group c), DGL-FA-ASODN-Cy5.5 (group d), DGL-FA-ASODN-Cy5.5-DCA (group e) and GEL-DGL-FA-ASODN-Cy5.5-DCA (group f) were given intravenously with a dosage of 0.195 mg ASODN-Cy5.5 per kg body weight by tail vein, respectively. The mice were anesthetized by an intraperitoneal injection of 0.16 ml 1% pelltobarbitalum natricum at 24 h post administration. The fluorescent distribution in whole body was observed through an *in vivo* imaging system (IVIS Lumina II, USA) with an excitation wavelength of 675 nm and an emission wavelength of 695 nm. After that, the mice were sacrificed, the major organs (heart, liver, spleen, lung and kidney) and tumor tissues were removed, washed with sterile PBS and immediately imaged.

### 2.12. *In vivo anti-tumor efficacy study*

Forty-two H22 tumor-bearing mice were randomly divided into six groups ($n = 7$ per group). The mice from therapeutic groups were treated with 0.2 ml of free ASODN, DGL-ASODN, DGL-FA-ASODN, DGL-FA-ASODN-DCA and GEL-DGL-FA-ASODN-DCA with a dosage of 5 mg ASODN per kg body weight by tail vein injection, respectively. The mice from control group were treated with saline. The treatment was carried out every other day for 14 d. And in this period, the body weight and tumor size of the mice were monitored and recorded every day. After 14 d, the mice were euthanized. The tumors were quickly removed. And the tumors were weighed after the blood on the surface was washed away with PBS. The tumor inhibit rate (TIR) was calculated according to the following formula [58].

$$\text{Tumor inhibitory rate (\%)} = \frac{\text{average tumor mass in control group} - \text{average tumor mass in therapeutic group}}{\text{average tumor mass in control group}} \times 100\%$$

### 2.13. *Statistical analysis*

All the data were statistically analyzed using software SPSS 17.0. And all results were expressed as mean ± standard deviation (SD). Meanwhile, the univariate ANOVA was used for statistical test. $P < 0.05$ indicated significant difference.

## 3. Results and discussion

### 3.1. *Preparation of step-by-step nanocomposites*

The preparation of ASODN-loaded nanocomposites was divided into the following five steps. Firstly, DGL-PEG-$NH_2$-Fmoc and FA-PEG-DGL-PEG-$NH_2$-Fmoc composites (abbreviated as DGL-$NH_2$ and DGL-$NH_2$-FA) were synthesized by conjugating the amino groups of DGL with the carboxyl groups of Fmoc-$NH_2$-$PEG_{2000}$-COOH and FA-$PEG_{2000}$-COOH under the catalysis of EDAC and NHS, respectively. The products were verified by FTIR. Secondly, ASODN was bound to DGL-$NH_2$ and DGL-$NH_2$-FA by electrostatic attraction to obtain products DGL-$NH_2$-ASODN and DGL-$NH_2$-FA-ASODN, respectively. The binding capacity of DGL-$NH_2$ and DGL-$NH_2$-FA with ASODN was verified by electrophoretic mobility shift assay (EMSA). In the third step, DGL-$NH_2$-ASODN-DCA and DGL-$NH_2$-FA-ASODN-DCA composites (abbreviated as DGL-ASODN-DCA and DGL-FA-ASODN-DCA) were synthesized by amide reaction between the amino groups of DGL and the carboxyl groups of DCA (Fig. 1). Zeta potentials of the products were monitored at pH 7.4, 6.8 and 5.0 to evaluate their sensitivity to pH of the medium. Agarose gel retardation assay was carried out to detect whether the modification of DCA affected the stability of ASODN. In the fourth step, GEL nanoparticles were synthesized by a two-step desolvation method optimized by us according to the previous literature [57]. The measures optimized were as follows. GEL concentration was reduced from 25 to 9.6 g/l. The crosslinking reaction time was prolonged from 30 min to 7.5 h. According to the method optimized, the particle size of the resultant gelatin nanoparticles reached an ideal range of about 97–102 nm, and decreased by about 2.8 times compared to the traditional method [57]. The final step, the ideal GEL nanoparticles were used as an inner core to provide a platform for grafting DGL-FA-ASODN-DCA, DGL-FA-ASDON, and DGL-ASDON-DCA composites. The final products (GEL-DGL-FA-ASODN-DCA, GEL-DGL-FA-ASDON and GEL-DGL-ASDON-DCA) were also subjected to EMSA to detect whether the combination of GEL affected the stability of ASODN.

### 3.2. *Characterization*

The morphologies and the corresponding size distributions of DGL-FA-ASODN-DCA, GEL, and GEL-DGL-FA-ASODN-DCA were characterized by TEM and DLS. Fig. 2A shows that DGL-FA-ASODN-DCA nanocomposite was homogeneous dispersion and spherical in shape. There was a significant difference in size distribution measured by TEM and DLS. The mean particle diameter was 10 nm on the basis of TEM, while this value was approximately 14–20 nm by DLS, which could be attributed to different sample states. The samples were observed in a dehydrated state by TEM, while were tested in an aqueous solution by DLS. According to TEM in Fig. 2B, the GEL were spherical nanoparticles with a compact structure, and the particle size was similarly much smaller compared to diameter (97–102 nm) measured by DLS. TEM images in Fig. 2C revealed that the final product (GEL-DGL-FA-ASODN-DCA) was some large spherical particles that had good dispersity and compact surface. Based to the DLS data (Fig. 2C), the GEL-DGL-FA-ASODN-DCA nanocomposite exhibited a distinguished increase in diameter with the range of about 170–192 nm, showing that DGL-FA-ASODN-DCA composite was successfully conjugated with GEL nanoparticles.

Fig. 2D demonstrated the FTIR spectra of DGL, DGL-$NH_2$ and DGL-$NH_2$-FA. DGL is a lysine polymer which contains a large amount of amino groups and amide bonds. As shown

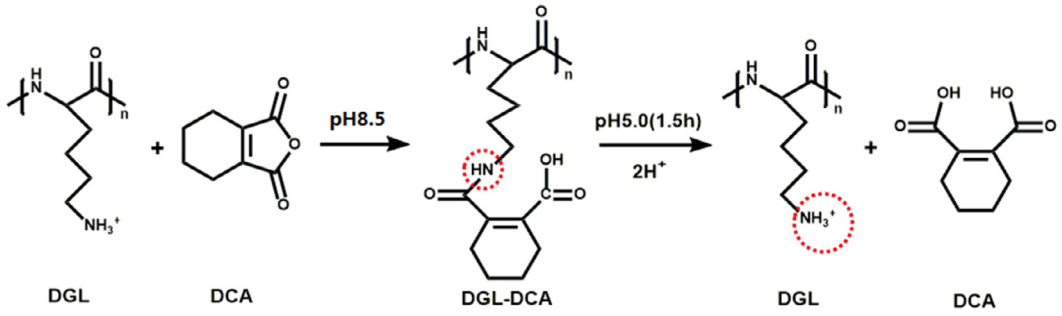


**Fig. 1 – The formation and breakage of pH-sensitive β-carboxylic amide bond between DGL and DCA.**

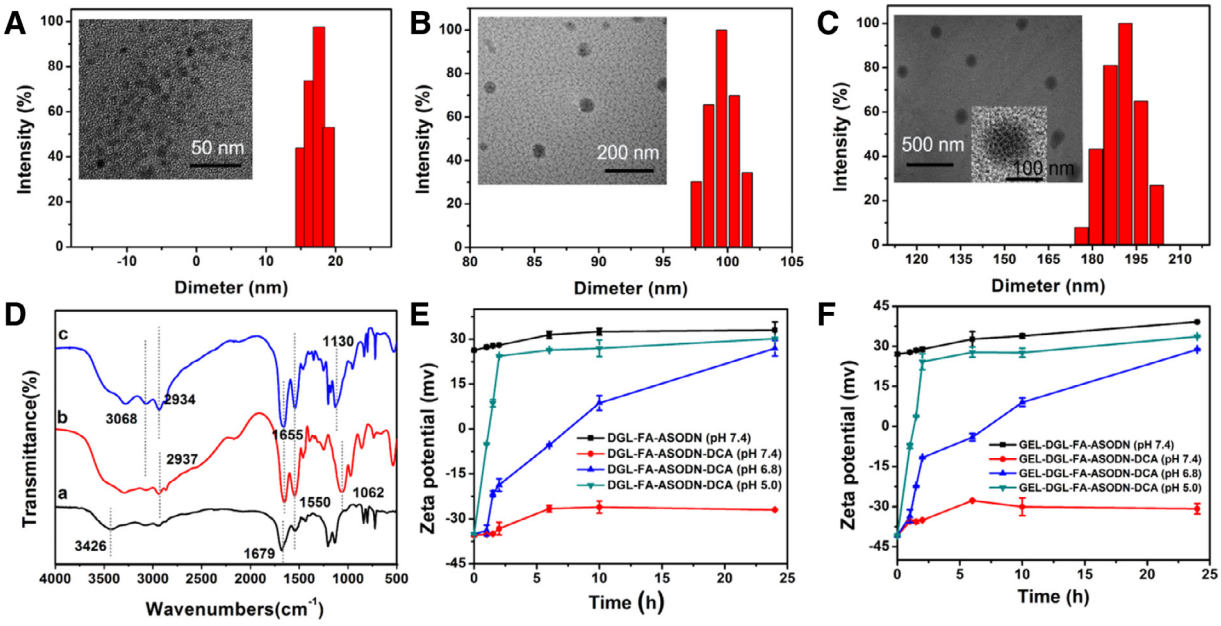


**Fig. 2 – The images and the corresponding size distributions of DGL-FA-ASODN-DCA (A), GEL (B), and GEL-DGL-FA-ASODN-DCA (C) were characterized by TEM and DLS, respectively; (D) FTIR of DGL (a), DGL-$NH_2$ (b), DGL-$NH_2$-FA (c); (E) Zeta potentials of DGL-FA-ASODN at pH 7.4, and DGL-FA-ASODN-DCA at pH 7.4, 6.8 and 5.0, respectively; (F) Zeta potentials of GEL-DGL-FA-ASODN at pH 7.4, and GEL-DGL-FA-ASODN-DCA at pH 7.4, 6.8 and 5.0, respectively. The data are expressed as mean ± SD ($n = 3$).**

in Fig. 2D-a, there were three peaks at 3426 $cm^{-1}$, 1679 $cm^{-1}$ and 1550 $cm^{-1}$ corresponding to the N–H stretching vibration of free amino groups, C=O stretching vibration of amide groups (amide I band) and N–H bending vibration of amide groups (amide II band), respectively, verifying that it is DGL. Compared with the spectra of DGL, two new characteristic peaks occurred at 1062 $cm^{-1}$and 2937 $cm^{-1}$, which was assigned to the C–O–C and C–H in PEG from Fmoc-$NH_2$-$PEG_{2000}$-COOH (Fig. 2D-b). Furthermore, the other two peaks at 1655 $cm^{-1}$ (amid I band) and 1550 $cm^{-1}$ (amide II band) became stronger (Fig. 2D-b), confirming that the CO–$NH_2$ groups between the carboxyl groups of Fmoc-$NH_2$-$PEG_{2000}$-COOH and amino groups of DGL have been formed. These results consistently indicated the successful synthesis of DGL-$NH_2$. According to the Fig. 2D-c, the spectra displayed the absorption peaks at 3068 $cm^{-1}$ and 2934 $cm^{-1}$ related to the C–H and =C–H from benzene rings deriving from FA molecule, while the absorption peaks at 1130 $cm^{-1}$ was assigned to the C–O–C of PEG from FA-PEG-COOH. Two peaks at 1655 $cm^{-1}$ (amide I band) and 1550 $cm^{-1}$ (amide II band) were stronger than in above two spectra. All of these results showed that the FA-PEG-COOH successfully combined with DGL-$NH_2$ (The product was abbreviated as DGL-$NH_2$-FA).

To observe the stability of DCA binding with nanocomposites in normal physiological, tumor and lysosomal environments, respectively, the zeta potentials of these composites were measured at pH 7.4, 6.8 and 5.0. As could be seen in Fig. 2E, in the medium of pH 7.4, the zeta potential of DGL-FA-ASODN composite was not only very high, being about +29 mV, but also stable within 24 h. This high positive charge value was mainly contributed by the positively charged amino groups of DGL. Zeta potential of DGL-FA-ASODN-DCA, however, dropped significantly at pH 7.4, and stabilized at the platform value of −28 mV during 7.5–24 h. This was because a large number of negatively charged carboxyl groups derived from DCA were introduced into the

DGL-FA-ASODN-DCA nanocomposite. When the pH values of media were reduced from 7.4 to 6.8 and 5.0, the zeta potential of DGL-FA-ASODN-DCA had a significant negative correlation with pH values and dramatically increased, especially at pH 5.0, the charges returned to the positive values at 1.5 h, and rose to the platform of +25 mV at 2.5 h. This value was close to that of DGL-FA-ASODN, reflecting the vast majority of DCA moiety has fallen off from DGL-FA-ASODN-DCA composite at pH 5.0. This could be attributed to the acid sensitivity of the $\beta$-amide bonds formed between DGL and DCA. When the DCA was removed from the nanocomposites in an acidic environment, the amino groups of DGL were exposed and reabsorbed protons to carry positive charges. Therefore, DCA could reversibly block amino groups of the DGL on DGL-FA-ASODN-DCA with the change of pH value. Fig. 2F showed the zeta potentials of GEL-DGL-FA-ASODN-DCA nanocomposite at different pH values. Firstly, the zeta potential of GEL-DGL-FA-ASODN at pH 7.4 was taken as a reference. This value was about +31 mV, and was close to that of DGL-FA-ASODN at pH 7.4, showing that grafting DGL-FA-ASODN onto the gelatin cores hardly changed the charge properties. Secondly, the zeta potential of GEL-DGL-FA-ASODN-DCA at pH 7.4 sharply decreased to the platform value of about −29 mV, which was attributed to the introduction of negative charge carboxyl groups of DCA. In addition, as the pH value of the medium decreased, the zeta potential of GEL-DGL-FA-ASODN-DCA significantly increased. At pH 5.0, the zeta potential returned to positive charge at 1.5 h and maintained a trend of continuous increase within 24 h, indicating that the DCA on nanocomposite was unstable in an acidic environment so that amino groups of DGL were free again and reabsorbed protons. This provided the basis for triggering the proton sponge effect in the lysosome.

### 3.3. *Agarose gel retardation assay*

One of the important performances of nanocarriers used for gene delivery is their efficient loading capacity. In order to evaluate the loading capacity and binding stability of the ASODN on vectors, an agarose gel retardation assay was carried out (Fig. 3). Free electronegative ASODN migrated to the positive pole in the electric field, and its migration distance was inversely proportional to the logarithm of its molecular mass. On the contrary, the migration of the nanocomposites would be retarded in the agarose gel due to large particles, and the moving distance towards the positive pole would be correspondingly shortened. In this study, the optimum mass ratio of DGL-$NH_2$ to ASODN was firstly determined by agarose gel retardation assay so as to provide the basis for a series of subsequent synthesis of ASODN-vector nanocomposites. As shown in Fig. 3A, free ASODN and empty DGL-$NH_2$ nanoparticles were assayed as controls in lane 1 and lane 2, respectively. The migration of free ASODN in the gel was not blocked, and it could be clearly seen that a bright ASODN band migrated to the positive pole, while the empty DGL-$NH_2$ nanoparticles in lane 2 has no migrating strand. Next, the DGL-$NH_2$-ASODN composites synthesized at different mass ratios of DGL-$NH_2$ to ASODN (1, 2, 4, 6, 8, 10, 12, 14 and 16, w/w) were added to the corresponding lanes for gel electrophoresis. As can be seen in lane 3 (Fig. 3A), when the mass ratio of DGL-$NH_2$ to ASODN was one, a weak ASODN band migrating to the positive pole could still be seen in gel, indicating that ASODN was excessive under this ratio, and the unbounded ASODN escaped. When the mass ratio of DGL-$NH_2$ to ASODN was equal to or greater than 2 in lane 4–11, no ASODN bands were detected, indicating that ASODN bound completely to the vectors. According to the previous literature [59], generally speaking, when the mass ratio of vector to ASODN was greater than 2, ASODN could be fully loaded.

On the one hand, as described above, the synthesis of the entire gene delivery system comprised four steps. After ASODN was combined with DGL-$NH_2$, there were still two important synthesis steps, namely: preparation of DGL-$NH_2$-ASODN-DCA (DGL-$NH_2$-FA-ASODN-DCA) and GEL-DGL-FA-ASODN-DCA (GEL-DGL-FA-ASDON and GEL-DGL-ASDON-DCA). It was necessary to stir in solution for a long-time during synthesis. In order to prevent the early release of the ASODN from the nanocomposites, the physical adsorption during uploading of ASODN should be avoided as much as possible. On the other hand, it should be pointed out that ASODN was just fully bound with nanocomposites when the mass ratio of DGL-$NH_2$ to ASODN was 2:1. ASODN was mainly uploaded in the form of electrostatic attraction. But the form of physical adsorption was cannot completely excluded. The latter had far less tight binding force than the former. When the mass ratio of ASODN was reduced in mixture, the physical adsorption would be greatly decreased. According to our trials, the mass ratio of 6:1 (DGL-$NH_2$ to ASODN) was proved to be the best formulation. This ratio has also been reported in the previous literature [59]. Therefore, in this study, DGL-$NH_2$ was mixed with ASODN at the mass ratio of 6:1 in the following synthesis for better combination, namely, the loading amount of ASODN on end product was 166.7 mg/g for GEL-DGL-FA-ASODN-DCA nanocomposite. Subsequently, it was further verified whether the following series of modifications on DGL-$NH_2$-ASODN would affect the stability of ASODN. As can be seen in Fig. 3B, free ASODN in lane 1 and DGL-$NH_2$-ASODN in lane 2 were taken as the positive and negative controls, respectively. The samples in the lane 3–5 were the mixed solutions after different fabrications such as binding of ASODN, modification of DCA and grafting of GEL, respectively. There were no ASODN bands in the lane 3–5 corresponding DGL-$NH_2$-FA-ASODN, DGL-$NH_2$-FA-ASODN-DCA, and GEL-DGL-FA-ASODN-DCA suspensions. These findings indicated that ASODN was stable on nanocomposites synthesized at the ratio of 6:1. Simultaneously, it was also confirmed that the resultant nanocomposites could be used as the vectors of gene delivery.

### 3.4. *Cellular uptake measurements*

In terms of growth characteristics of cultured cells *in vitro*, HepG2 cells and Hela cells belong to adherent growth. When *in vitro* cellular uptake and cytotoxicity were measured, the adherent cells were easy to be detected and observed. In order to observe the distinction in cellular uptake and cytotoxicity between hepatoma carcinoma cells and other cancer cells, cervical cancer Hela cells were also selected as a model in this work. Cellular uptake behaviors of GEL-DGL-FA-ASDON-DCA, GEL-DGL-FA-ASDON, GEL-DGL-ASDON-DCA, DGL-FA-ASODN-

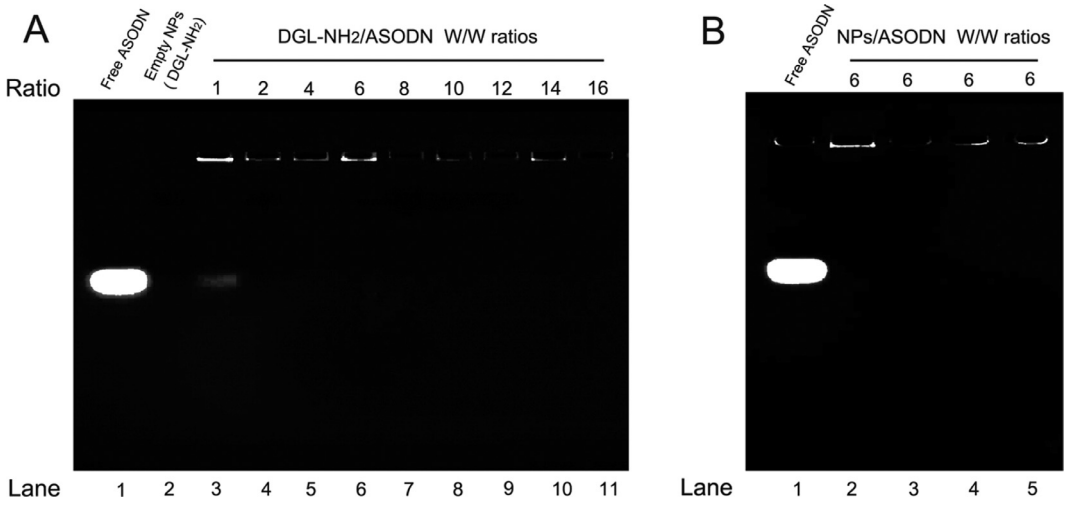


**Fig. 3 – (A) Agarose gel retardation assay of nanoparticles prepared at various mass ratios of DGL-NH2 to ASODN (1, 2, 4, 6, 8, 10, 12, 14 and 16, w/w). (B) Agarose gel retardation assay of nanoparticles prepared at mass ratio of 6:1 (vector: ASODN), Lane 1:Free ASODN; Lane 2: DGL-NH2-ASODN; Lane 3: DGL-NH2-FA-ASODN; Lane 4: DGL-NH2-FA-ASODN-DCA; Lane 5: GEL-DGL-FA-ASODN-DCA.**

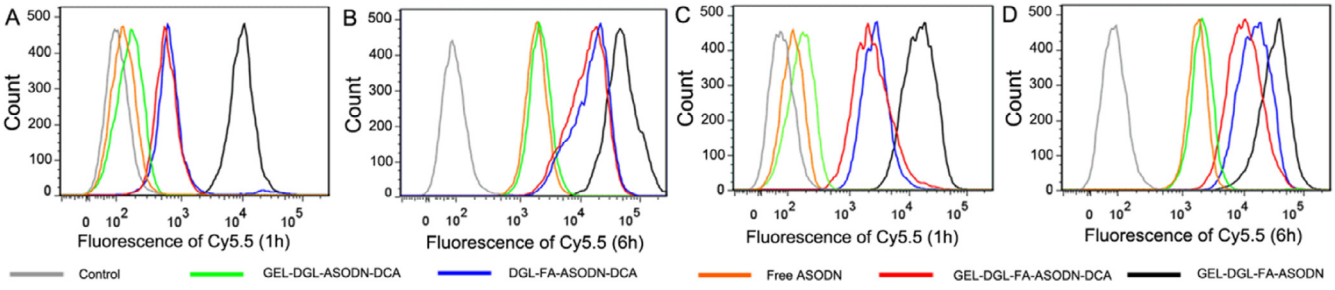


**Fig. 4 – Cellular uptake behaviors of GEL-DGL-FA-ASDON-DCA, GEL-DGL-FA-ASDON, GEL-DGL-ASDON-DCA, DGL-FA-ASODN-DCA, and free ASODN in HepG2 cells at 1 h (A) and 6 h (B) and in HeLa cells at 1 h (C) and 6 h (D).**

DCA, and free ASODN in HepG2 and HeLa cells were presented in Fig. 4. The ASODN was labeled with Cy5.5 to assay cellular uptake. The fluorescence intensity within the HepG2 and HeLa cells treated with different nanocomposites or free ASODN for 1 h or 6 h were measured by flow cytometry, respectively. The cells without treatment were used as a control. It can be seen that the fluorescence in HepG2 or HeLa cells was the lowest in free ASODN group at not only 1 h but also 6 h (Fig. 4). It was the negative charge that ASODN was poorly taken up by cells [60]. On the contrary, HepG2 and HeLa cells treated with GEL-DGL-FA-ASODN possessed always the strongest fluorescence in all groups at 1 h or 6 h. In addition to the FA receptor-mediated endocytosis, a major reason was why GEL-DGL-FA-ASODN carried high positive charges (Fig. 2F). More specifically, at 1 h, the fluorescence intensities within HepG2 and HeLa cells treated with GEL-DGL-FA-ASDON-DCA, GEL-DGL-ASDON-DCA, and DGL-FA-ASODN-DCA were much lower than that with GEL-DGL-FA-ASDON (Fig. 4A), which might be because the former three nanocomposites with negative surface charges derived from DCA induced the electrostatic repulsion with negatively charged cell membranes, thus, the vectors were not apt to be endocytosed by cells. This repulsive interaction was dominant within the first 1 h, by contrast, the FA receptor-mediated endocytosis was subordinate. When the incubation time of the nanocomposites with cells was extended to 6 h, the fluorescence intensities within the cells were obviously increased. Further comparison found that the fluorescence intensity within the cells treated with GEL-DGL-FA-ASODN-DCA was slightly weaker than that with DGL-FA-ASODN-DCA (Fig. 4B), reflecting that the grafting of DGL-FA-ASODN-DCA on GEL nanoparticle had a bit influence on the cellular uptake. However, the uptake amount of GEL-DGL-FA-ASODN-DCA by cells was observably higher than that of GEL-DGL-ASDON-DCA, indicating that the FA receptor-mediated endocytosis became the preponderant at 6 h. All of these results suggested that GEL-DGL-FA-ASODN-DCA could effectively carry ASODN into cells by FA receptor-mediated endocytosis at 6 h.

### 3.5. *Lysosomal escape capacity evaluation*

It is known that the successful lysosome escape is crucial for high-efficient gene delivery [61]. In order to test whether introduction of DCA moieties could enhance the lysosomal escape ability of gene delivery systems, the intracellular

distributions of the nanocomposites were traced with time by using Cy5.5 fluorescein-labeled ASODN (red) on CLSM. Late endosomes or lysosomes were stained with LysoTracker Green DND-26 (green), and nucleus was stained with DAPI (blue) to identify the localization of these organelles. The co-localization of ASODN-loaded nanocomposites with lysosomes generated a yellow fluorescence in merged images.

Fig. 5A and 5B showed that the subcellular distribution of GEL-DGL-FA-ASODN-DCA and GEL-DGL-FA-ASODN in HepG2 cells at 1, 2, 4, and 6 h, respectively. It was clearly observed that the red fluorescence of GEL-DGL-FA-ASODN-DCA and GEL-DGL-FA-ASODN groups increased with time under Cy5.5 excitation, reflecting that the amount of nanocomposites entering the cell increased because the FA receptor-mediated endocytosis dominated gradually with time. Further comparison revealed that the red fluorescence of GEL-DGL-FA-ASODN-DCA in the cells was slightly inferior to GEL-DGL-FA-ASODN at each time point under Cy5.5 excitation light (Fig. 5A and 5B). Although they were similarly mediated by FA receptor, there was a subtle difference in the amount of entering cells because GEL-DGL-FA-ASODN-DCA carried negative charge, while GEL-DGL-FA-ASODN possessed positive charge in pH7.4 medium (Fig. 2F). However, over time, it could be seen in the merged images (D + C + L) that the red fluorescent intensity of GEL-DGL-FA-ASODN-DCA was significantly higher than that of GEL-DGL-FA-ASODN (Fig. 5A and 5B), especially at 6 h. This may be because when GEL-DGL-FA-ASODN-DCA was transferred into the lysosome, the amide bond of DCA was broken due to its sensitivity to acid, triggering the proton sponge effect and escaping from the lysosome into the cytoplasm. Furthermore, the green fluorescence of GEL-DGL-FA-ASODN-DCA group became weak at 4 h, and basically disappeared at 6 h. This was because the lysosome has shown the tendency of rupture, and could not fully be dyed by Lyso-Tracker -Green, which green fluorescent signal representing lysosomes was almost invisible. And the yellow fluorescence could hardly be seen except red and blue fluorescence in the merged images, showing most of the GEL-DGL-FA-ASODN-DCA nanocomposites released into the cytoplasm. Therefore, the red fluorescence of GEL-DGL-FA-ASODN-DCA group in the cytoplasm increased (Fig. 5A). By contrast, GEL-DGL-FA-ASODN showed a large amount of yellow fluorescence in the merged image at 6 h (Fig. 5B), which was the color of the overlapping of the red nanocomposites with the green lysosome, indicating that GEL-DGL-FA-ASODN was trapped in the lysosome. This difference of the subcellular distributions between GEL-DGL-FA-ASODN-DCA and GEL-DGL-FA-ASODN confirmed that the modification of DCA on the nanocomposite could promote the escape from the lysosome. According to the previous literatures [25,26], when PEI and PAMAM were assembled into vectors for gene delivery, non-protonated amines on these cationic dendrimers triggered the proton sponge effect by absorbing protons in the lysosomes, and promoted lysosomal escape. In the present study, the lysosomal escape could similarly be achieved by grafting acid sensitive bonds on DGL.

In addition, the intracellular red fluorescence in DGL-FA-ASODN-DCA group (Fig. 5C-a) was slightly higher than that in GEL-DGL-FA-ASODN-DCA (Fig. 5A) under Cy5.5 excitation at 6 h. Although all of them relied on folate receptor-mediated endocytosis, the particle size of DGL-FA-ASODN-DCA was about 10 times smaller than that of GEL-DGL-FA-ASODN-DCA, so the resistance encountering for the former was less than the latter when entered the cells by passive endocytosis, and the amount of cells entering was relatively large [62]. At the same time, it was found in the merged images that DGL-FA-ASODN-DCA group had a large amount of red fluorescence (Fig. 5C-a), indicating that the nanocomposites escaped basically from lysosome at 6 h under the triggering of DCA. This proved the role of DCA again.

In the case of GEL-DGL-ASODN-DCA nanocomposites, there were only amount of red fluorescence under Cy5.5 excitation light, and it is similar condition in the merged image (Fig. 5C-b). These results indicated that the negative charges and the lack of folate on the vectors resulted in a significant reduction in the amount of nanocomposites entering into the cells. But, once they were endocytosed by the cells, the GEL-DGL-ASODN-DCA nanocomposites could escape from lysosomes under DCA triggering, so there is a small amount of red fluorescence in the cytoplasm (merged image). Finally, it was found that the red free ASODN overlapped with the green lysosomes became the yellow color in the merged image of the intracellular localization of the cells (Fig. 5C-c), and the red fluorescence was hardly seen in the cytoplasm. This demonstrated that free ASODN was trapped in the lysosome and could not successfully enter the cytoplasm [3,14,63].

### 3.6. *In vitro cytotoxicity*

The cytotoxicity of free ASODN and ASODN-loaded nanocomposites with a series of concentrations at pH 7.4 and at 24 h were evaluated in hypoxia HepG2 and HeLa cells by MTT assay. As shown in Fig. 6, the trend of cell viability was the same after HepG2 and HeLa cells were incubated with different nanomaterials. Firstly, empty GEL-DGL-FA-DCA nano-vectors showed high cell viability for HepG2 and HeLa cells (>90%) even at a high concentration of 100 μg/ml, indicating that the empty vectors possessed relatively good biocompatibility. The empty GEL-DGL-FA-DCA nanocomposites had a negative charge surface derived from DCA, resulting in a minimal cytotoxicity. The PEI and PAMAM were often used as classical vectors that could escape from the lysosomes because of the mechanism known as the 'proto-sponge' effect [3]. However, the direct use of these cationic dendrimers possessed fairly high toxicity due to large amount of positive charges and their non-biodegradability [27,64]. In the present study, using DCA to block reversibly the cationic DGL, it could similarly exert the proton sponge effect. Furthermore, the DGL is highly biocompatible and biodegradable material, and the degradation product lysine is nontoxic. Thus, the toxicity of the vectors was greatly reduced. Secondly, although the cell viability of the free ASODN group was slightly lower than that of the empty vector group, these values were still as high as 67% and 65.7% for HepG2 and HeLa cells when the free ASODN concentration reached 100 μg/ml. The electronegative molecules of free ASODN generated electrostatic repulsion with the cell membrane, preventing it from getting into the cells [60]. Even if a small amount of

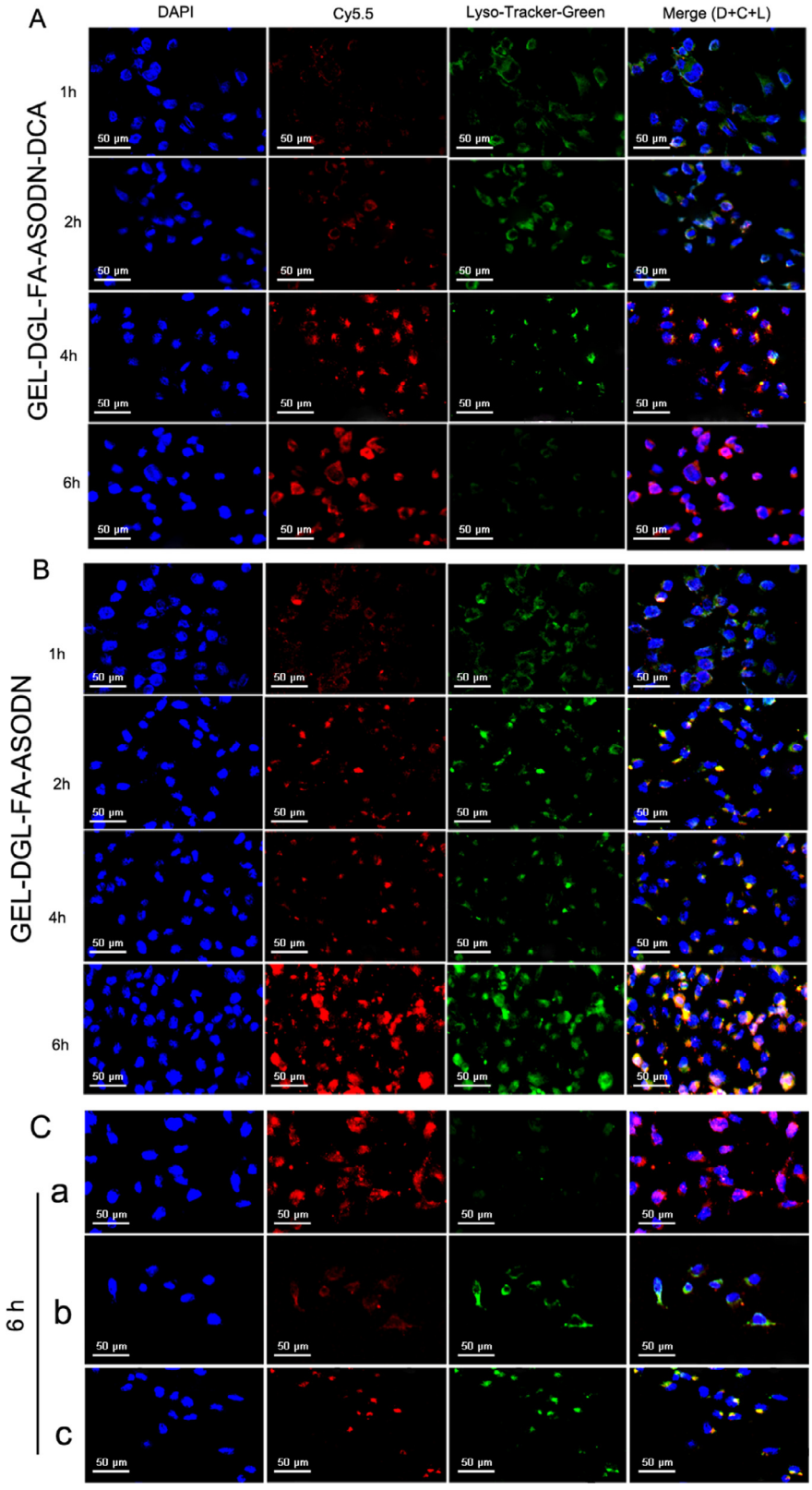


**Fig. 5 – The subcellular distribution of GEL-DGL-FA-ASODN-DCA (A), GEL-DGL-FA-ASODN (B), DGL-FA-ASODN-DCA (C-a), GEL-DGL-ASODN-DCA (C-b), and free ASODN (C-c) in HepG2 cells at different time.**

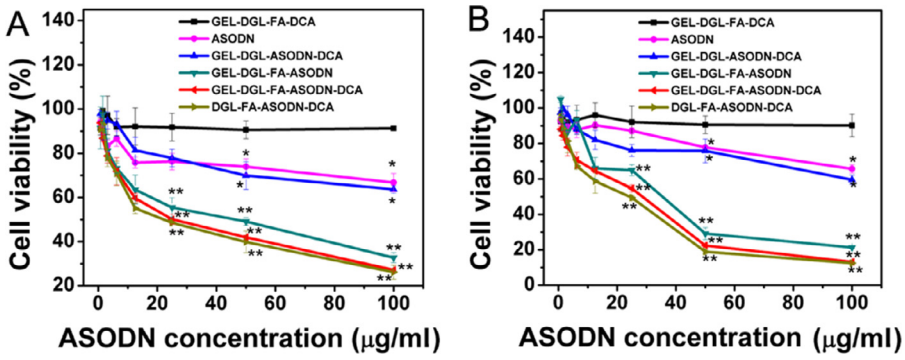


**Fig. 6 – Relative cell viabilities of hypoxia HepG2 (A) and HeLa (B) cells after incubated with various concentrations of free ASODN and ASODN loaded on GEL-DGL-ASODN-DCA, GEL-DGL-FA-ASODN, GEL-DGL-FA-ASODN-DCA, and DGL-FA-ASODN-DCA nanocomposites, and empty vector GEL-DGL-FA-DCA at pH 7.4 and at 24 h. The data are expressed as mean ± SD ($n = 3$). *$P < 0.05$ and **$P < 0.01$ *versus* GEL-DGL-FA-DCA group according to ANOVA.**

ASODN molecules got into the cell, they could not escape from the lysosomal compartment due to membrane barriers, and their fate would be degraded [63,65]. So, there was a relatively high level of cell viability. Thirdly, the cell viabilities of the ASODN-loaded nanocomposites decreased with the increase of ASODN content, showing an obvious dose-dependent cytotoxicity. The order of cell viabilities for two kinds of cells in these groups was as follows: GEL-DGL-ASODN-DCA >GEL-DGL-FA-ASODN > GEL-DGL-FA-ASODN-DCA> DGL-FA-ASODN-DCA (Fig. 6). Compared with GEL-DGL-ASODN-DCA, GEL-DGL-FA-ASODN exerted more cytotoxicity on cells due to the mediation of folate receptors. When GEL-DGL-FA-ASODN further conjugated with DCA moiety, the resultant GEL-DGL-FA-ASODN-DCA nanocomposite could trigger a proton sponge effect in the lysosomes, so that ASODN escaping from the lysosomes into the cytoplasm could interact with the target genes and induced cell apoptosis to the maximum extent. So, GEL-DGL-FA-ASODN-DCA had stronger the inhibition ability of cells growth than GEL-DGL-FA-ASODN. However, it was found that the DGL-FA-ASODN-DCA with a particle size 10 times smaller than GEL-DGL-FA-ASODN-DCA had more cytotoxicity on cells, which may be due to the fact that the small particles were more likely to be endocytosed into the cells [62].

Furthermore, it can be seen in Fig. 6 that the cytotoxicity of the FA-modified nanocomposites in HeLa cells was stronger than in HepG2 cells. For example, when the concentration of ASODN reached 100 μg/ml, the cell viability of the GEL-DGL-FA-ASODN-DCA nanocomposite in HepG2 cells was 27.2% (Fig. 6A), while this value was only 13.1% in HeLa (Fig. 6B).

In general, the cytotoxicity of nanomaterials was determined in the media of pH 5.0, pH 6.8, and pH 7.4. However, in this study, according to the zeta potential characterization, it has been proved that the amide bonds between DCA and DGL could easily break off at pH 5.0 (Fig. 2E and 2F), so the DCA-unbound GEL-DGL-FA-ASODN nanocomposite was directly selected to measure cell viability at pH 7.4. Furthermore, in the medium of pH 6.8, the results of zeta potential measurement showed that it would take 7.5 h to break the amide bond between DCA and DGL. On the basis of the cellular uptake imaging (Fig. 5), the nanocomposites have been endocytosed into the cells when the cells were incubated with material for 2 h, which was consistent with the literatures [66–68]. It was this time difference that makes these nanocomposites in pH 6.8 media have little effect on cell viabilities. At the same time, the cytotoxicity induced by nanocomposites has not only dose-dependent effect, usually but also time-dependent effect. However, the cytotoxicity induced by these materials within 24 h showed a similar trend with the change of concentration. So *in vitro* cytotoxicity in this study was only evaluated at pH 7.4 and 24 h point.

### 3.7. *HIF-1α mRNA level analysis*

qRT-PCR was used to detect the effect of ASODN-loaded nanocomposites on HIF-1α mRNA expression level in its transcription process, in turn, to investigate whether the vector developed could mediate gene internalization, trigger lysosomal escape and deliver ASODN to target genes, so as to further clarify the feasibility of gene therapeutics. In this study, $CoCl_2$ was used to stimulate HepG2 cells to construct a hypoxia model, so that the mRNA of the HIF-1α target gene was highly expressed. And then the HepG2 cells were incubated with free ASODN or ASODN-loaded nanocomposites with 0.8 μg/ml of ASODN concentration for 12 h, and the expression level of the target gene mRNA was detected by qRT-PCR. As shown in Fig. 7, the Control represented a negative control group without any treatment, and the expression level of its HIF-1α mRNA was used as the comparison object of each experimental group. Group A was the positive control group without any treatment after $CoCl_2$ stimulation. As can be seen in Fig. 7A, the mRNA expression of the positive control group was 3.23 times as high as that of the negative control group, indicating that $CoCl_2$ could induce up-regulation of HIF-1α mRNA level in cells, and the hypoxia model was successfully constructed. Fig. 7B demonstrated that compared with the positive control group, the mRNA expression of cells treated with free ASODN decreased to a certain extent, but the expression quantity was still about 2.8 times as high as that of the control group, which showed free ASODN could not effectively inhibit the expression of target gene mRNA. This was perhaps that

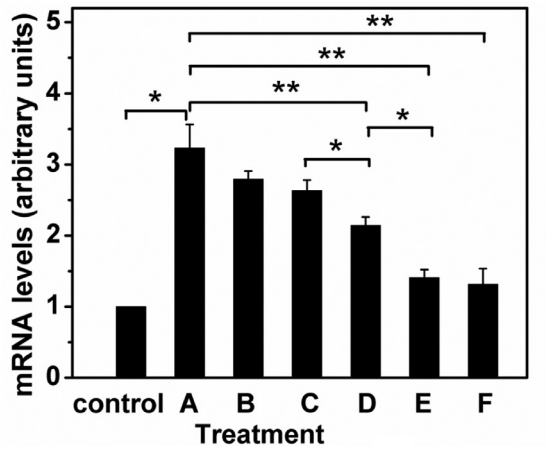


**Fig. 7 – Quantitative assay of HIF-1α gene expression in hypoxia HepG2 cells by qRT-PCR. Control was a negative control group without any treatment. (A) was the positive control group without any treatment after $CoCl_2$ stimulation. (B-F) were experimental groups treated with free ASODN (B), GEL-DGL-ASODN-DCA (C), GEL-DGL-FA-ASODN (D), GEL-DGL-FA-ASODN-DCA (E), and DGL-FA-ASODN-DCA (F) nanocomposites with 0.8 μg/ml of ASODN concentration for 12 h, respectively. The data are expressed as mean ± SD ($n = 3$). Statistical significances are *$P < 0.05$ and **$P < 0.01$.**

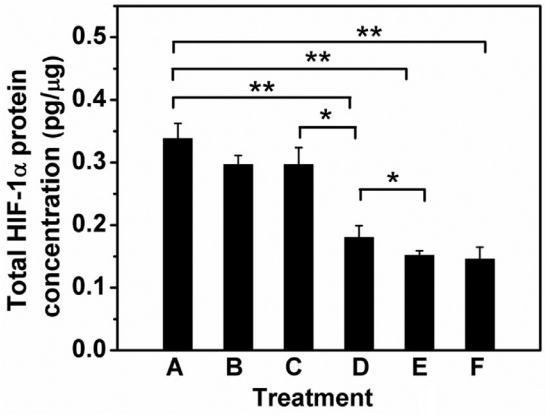


**Fig. 8 – Quantitative assay of HIF-1α protein concentrations in hypoxia HepG2 cells by ELISA. A was the positive control group without any treatment after $CoCl_2$ stimulation. B-F were experimental groups treated with free ASODN (B), GEL-DGL-ASODN-DCA (C), GEL-DGL-FA-ASODN (D), GEL-DGL-FA-ASODN-DCA (E), and DGL-FA-ASODN-DCA (F) nanocomposites with 0.8 μg/ml of ASODN concentration for 12 h, respectively. The data are expressed as mean ± SD ($n = 3$). Statistical significances are *$P < 0.05$ and **$P < 0.01$.**

negatively charged ASODN molecules were vastly prevented from cellular internalization, or trapped in lysosome and hydrolyzed by the enzymes. Compared with group B, the mRNA expression of cells treated with GEL-DGL-ASODN-DCA (group C) and GEL-DGL-FA-ASODN (group D) decreased to a certain extent, in particular, the decline was significant in group D, showing that the expression of target genes could be down-regulated through increasing the concentration of ASODN in tumor cells by the FA-mediating endocytosis. What was more, after the hypoxic cells were incubated with GEL-DGL-FA-ASODN-DCA, the HIF-1α mRNA expression was significantly downregulated by 57% compared with the positive control group, indicating that the target gene was effectively inhibited (group E). It is the recombination of ASODN uploaded onto the nanocomposites with the target gene that caused degradation of its mRNA by activated RNase H, thus reducing the HIF-1α mRNA level [13,15]. It was essential to endow the carrier with two functions in here: FA mediated cell internalization and DCA induced proton sponge effect. So, the resultant GEL-DGL-FA-ASODN-DCA nanocomposite has fulfilled its mission satisfactorily. When the cells were incubated with DGL-FA-ASODN-DCA, the down-regulation of HIF-1α mRNA expression was greater, was only 41% of the positive control group (group F), and the difference between group E and F was only their particle sizes, again proving that small particles were more likely to achieve cell internalization *in vitro*.

### 3.8. *Enzyme-linked immunosorbent assay (ELISA)*

In order to detect whether the ASODN-loaded nanocomposites could inhibit the expression of the HIF-1α protein in its translation process, the hypoxia HepG2 cells treated with free ASODN or ASODN-loaded nanocomposites for 12 h were lysed with RIPA lysis buffer. The HIF-1α protein from the total protein extracted was quantified by ELISA. The results were presented in Fig. 8. No HIF-1α protein was detected in the normoxic control group, indicating that HIF-1α protein expression was extremely weak in cells untreated, therefore, there was not datum in Fig. 8. But the cells exposed to $CoCl_2$ without any treatment (the positive control group A) had a high expression of HIF-1α protein (A), reflecting that $CoCl_2$ could stimulate the high expression of HIF-1α protein in cells. Furthermore, free ASODN (B) and GEL-DGL-ASODN-DCA nanocomposite (C) hardly inhibited the expression of HIF-1α protein, which may be because neither was effectively delivered to the targets. However, the cells treated with GEL-DGL-FA-ASODN (D), GEL-DGL-FA-ASODN-DCA (E), and DGL-FA-ASODN-DCA (F) nanocomposites showed significant lower expression of HIF-1α protein than group A. The total concentrations of HIF-1α protein only accounted for 53%, 44% and 43% of the positive control group (A), respectively, indicating that the FA- and DCA-modified nanocomposites inhibited the expression of the target protein by promoting the FA-mediated targeting and DCA-induced escaping ability.

According to the antisense strategies, the ASODN can not only directly destruct mRNA by RNase H which is activated by antisense-mRNA hybrids at the mRNA level but also down-regulate the translation of proteins by disturbing gene expression from mRNA at the protein level [15,69,70]. This study testified that the GEL-DGL-FA-ASODN-DCA nanocomposite can synchronously inhibited mRNA expression and HIF-1α protein translation. In other words, the GEL-DGL-FA-ASODN-DCA nanocomposite could achieve the tumor suppression at different levels. So, this is a kind of effective gene therapeutics.

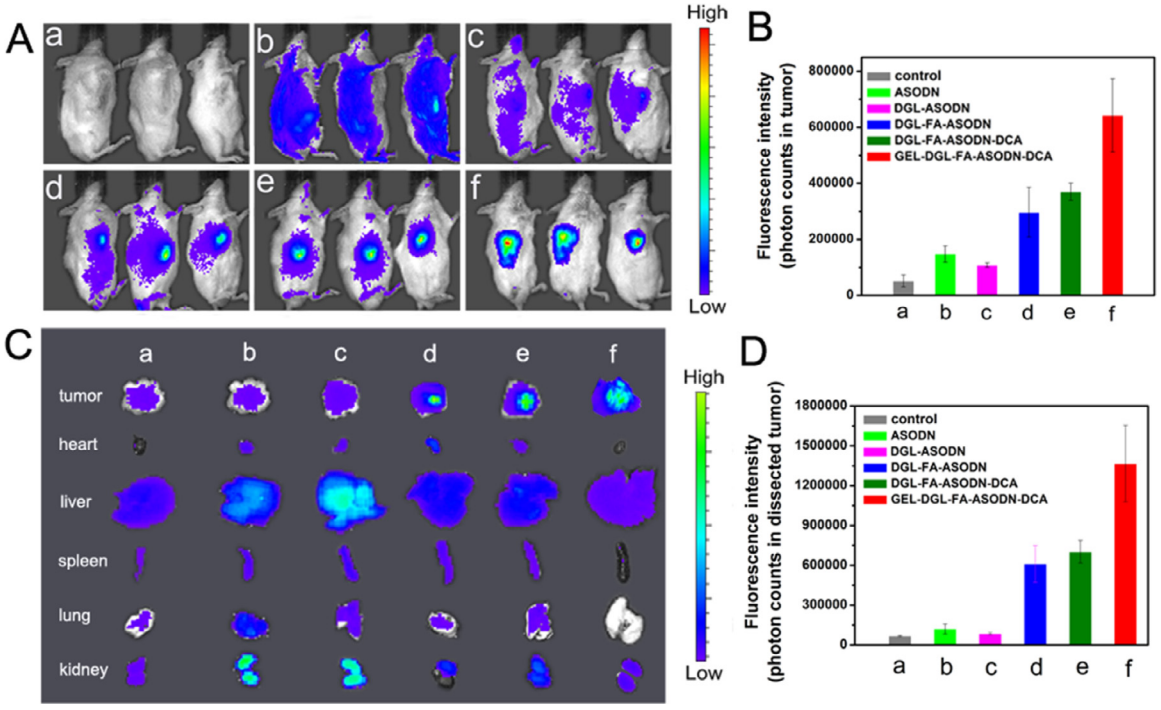


**Fig. 9 – (A) Typical *in vivo* optical images of male H22-bearing Kunming mice post-intravenous injection of saline (control group a), free ASODN (b), DGL-ASODN (c), DGL-FA-ASODN (d), DGL-FA-ASODN-DCA (e), and GEL-DGL-FA-ASODN-DCA (f) with a dosage of 0.195 mg ASODN–Cy5.5 per kg BW by tail vein, respectively. (B) Quantitative assay of the fluorescence intensity from the tumors of different groups based on *in vivo* optical images. (C) Optical images from the representative tissues from different groups. (D) Quantitative assay of the fluorescence intensity from dissected tumors. Images were taken using the IVIS Imaging System (IVIS Lumina II, USA) in anesthetized mice with 5% chloral hydrate at 24 h post administration. The system uses color coding of fluorescence with red coding for high levels of fluorescence and blue color for low levels. Excitation = 675 nm, emission = 695 nm. The data are expressed as mean ± SD ($n = 3$).**

### 3.9. *In vivo imaging analysis*

In terms of cell origin, HepG2 cells are human hepatocellular carcinoma cells, while H22 cells are mouse hepatocellular carcinoma cells. H22 is suspended growth cell. *In vivo* studies, in order to make it easier to build hepatocellular carcinoma model in mice, many researchers have used the H22 model and obtained excellent anti-cancer research results. Therefore, *in vitro* HepG2 and Hela cells were selected and *in vivo* H22 cells were used. To evaluate the targeting ability of ASODN-loaded nanocomposites in H22 tumor-bearing mice, the fluorescence distribution was observed using a small animal imaging system at 24 h after intravenous injection of Cy5.5-labeled nanocomposites. The concentrations, doses, route and frequency of nanocomposites administration were selected on the basis of the literature [71]. Fig. 9A shows the *in vivo* images of the mice treated with different formulations. Statistical quantification of the fluorescent photons in tumors from different groups based on *in vivo* optical images was shown in Fig. 9B. Saline group (a) had no fluorescence as a control. The fluorescence of free ASODN group had a wide distribution in the body as a whole (Fig. 9A-b), reflecting the non-specificity of free ASODN. Compared with free ASODN group, the mice displayed significant weak fluorescence in DGL-ASODN group (Fig. 9A-c and 9B-c). This was because DGL-ASODN nanocomposite was primarily positively charged so that it was easy to be removed by the red blood cells and albumin in the blood by electrostatic attraction as they circulated through the body [38]. Although the fluorescence intensity of DGL-FA-ASODN group (Fig. 9A-d) was also weak in the body as a whole, the fluorescence gradually accumulated in the tumor site (Fig. 9B-d), which could be interpreted as the folate-mediated targeting. It can also be clearly seen that abundant fluorescence was accumulated in tumors of the mice treated with DGL-FA-ASODN-DCA (Fig. 9A-e and 9B-e). This is mainly because the modification of DCA endowed nanocomposite with a large amount of negative charge on its surface, which may extend the circulation time by reducing the risk of removed from the blood. Moreover, the folate-mediated targeting accelerated the enrichment of more nanocomposites in the tumor sites. According to the results, the mice treated with GEL-DGL-FA-ASODN-DCA nanocomposite exhibited the strongest fluorescence in tumor sites in all groups (Fig. 9A-f and 9B-f), indicating GEL-DGL-FA-ASODN-DCA could be efficiently delivered to and concentrated in tumor site. It is reported that nano-sized agents with a diameter between 30 and 200 nm can prevent the kidney from excreting it and avoid the risk of being rapidly recognized and trapped by the reticuloendothelial system (RES) [72,73]. The GEL-DGL-

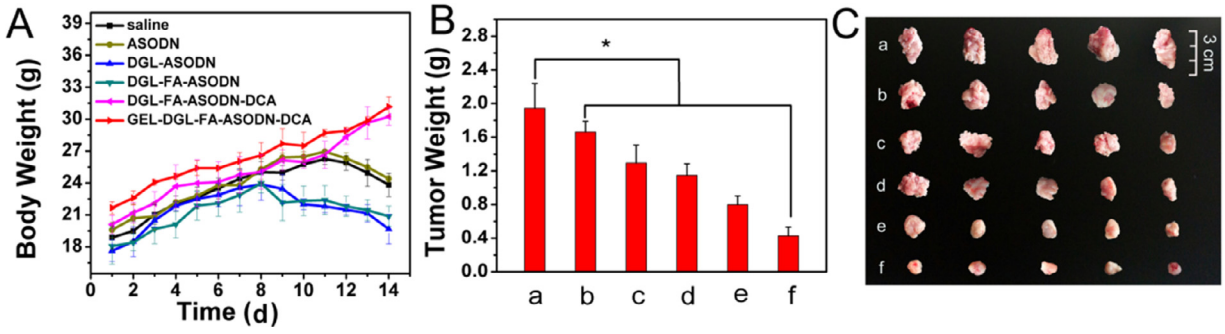


**Fig. 10 – *In vivo* antitumor efficacy after the treatment. The changes in body weight (A) and tumor weight (B) from H22 tumor-bearing Kunming mice treated with saline (a), free ASODN (b), DGL-ASODN (c), DGL-FA-ASODN (d), DGL-FA-ASODN-DCA (e), and GEL-DGL-FA-ASODN-DCA (f) with a dosage of 5 mg ASODN per kg BW by tail vein injection every other day for 14 d, respectively. (C) The photograph of the tumors separated from these mice. The scale bar in figure shows 3 cm. The data are expressed as mean ± SD ($n = 7$). *$P < 0.05$ *versus* control group according to ANOVA.**

FA-ASODN-DCA nanocomposite possessed a particle size of approximately 170–192 nm that was about 10 times as big as that of DGL-FA-ASODN-DCA (14–20 nm). Thus, GEL-DGL-FA-ASODN-DCA nanocomposite improved the aggregation in tumor site more than DGL-FA-ASODN-DCA by EPR effect [72]. This was achieved by adding a gelatin core inside the vector.

To more intuitively observe the accumulation of nanocomposites in the main organs, such as heart, liver, spleen, lung, kidney and tumor, the optical images of the tissues separated from different groups were acquired and the quantitative assay of the fluorescence intensity was achieved. As shown in Fig. 9C and 9D, on the one hand, the fluorescence signals in liver and kidney were higher than other normal tissues, especially, in liver and kidney of the free ASODN and DGL-ASODN groups. This showed that free ASODN and DGL-ASODN have potential toxicity and side effects on normal tissues, and the damages to liver and kidney were the greatest. On the other hand, in terms of the fluorescence intensity in the tumors (Fig. 9D), the GEL-DGL-FA-ASODN-DCA nanocomposite displayed the maximum distribution and was overwhelmingly accumulated in the tumor tissues (Fig. 9 D-f), further testifying its best specific targeting ability to tumor compared with other groups.

### 3.10. *In vivo anti-tumor efficacy study*

The anti-tumor efficacy *in vivo* was studied using H22 tumor-bearing mice. Free ASODN and different ASODN-carried nanocomposites were injected into the tail vein of mice every other day for 14 d. The mice from control group were treated with saline. The body weight and tumor size of the mice were observed and recorded every day. The dissected tumor was weighed and photographed after mice were sacrificed. As it was revealed in Fig. 10A, the body weight in the control and free ASODN groups continued to rise within 11 d, and then declined. This was because the rapid growth of the initial tumor in early days led to increase of the body weight, while the later progression of tumor affected the growth of the mice. The weight loss of mice in the DGL-ASODN and DGL-FA-ASODN groups was advanced to the 8 d (Fig. 10A), reflecting that these mice not only suffered from tumor, but also were exposed to the toxicity and side effects of the drug on normal tissues. It is gratifying that the weight of mice in the DGL-FA-ASODN-DCA and GEL-DGL-FA-ASODN-DCA groups continually increased throughout the treatment procedure (Fig. 10A). Especially, the weight of mice treated with GEL-DGL-FA-ASODN-DCA nanocomposite was higher than that with DGL-FA-ASODN-DCA, indicating that the former grew better than the latter. This may be because the tumor of the former was adequately suppressed. Further research found that the changes in the mass of tumors during treatment also supported this speculation. The tumor growth rates of mice treated with GEL-DGL-FA-ASODN-DCA and DGL-FA-ASODN-DCA nanocomposites were much lower than other experimental groups (Fig. 10B and 10C). Their tumor inhibitory rates were 77.99% and 58.99%, occupying 5.4 times and 4.1 times as high as that of free ASODN group (Table 1), respectively. Particularly, the GEL-DGL-FA-ASODN-DCA nanocomposite had the better tumor suppressive effect than DGL-FA-ASODN-DCA. Although *in vitro* analysis showed that the cellular internalization in DGL-FA-ASODN-DCA and GEL-DGL-FA-ASODN nanocomposites were slightly better than GEL-DGL-FA-ASODN-DCA according to the cellular uptake and

**Table 1 – The antitumor activities of ASODN, DGL-ASODN, DGL-FA-ASODN, DGL-FA-ASODN-DCA and GEL-DGL-FA-ASODN-DCA in H22 tumor-bearing male Balb/c mice.**

| Groups | Tumor weight (g) | TIR[a] (%) |
|---|---|---|
| Saline | 1.94 ± 0.29 | – |
| ASODN | 1.66 ± 0.12* | 14.48 |
| DGL-ASODN | 1.29 ± 0.21* | 33.47 |
| DGL-FA-ASODN | 1.14 ± 0.13* | 40.94 |
| DGL-FA-ASODN-DCA | 0.79 ± 0.10* | 58.99 |
| GEL-DGL-FA-ASODN-DCA | 0.43 ± 0.10* | 77.99 |

*Notes:* The data are expressed as mean ± SD ($n = 7$).
[a] Tumor inhibitory rate (TIR, W%) were calculated according to the tumor weight of mice treated with saline (control group).
* $P < 0.05$ *versus* control group according to ANOVA.

imaging, *in vivo* researches found GEL-DGL-FA-ASODN-DCA had better anti-tumor efficacy. Except that DCA achieved proton sponge effect, a main reason was that the introduction of gelatin core into the vector effectively improved the specific therapeutic effect of tumor by enhancing permeability and retention effect on the tumor site [72].

## 4. Conclusions

Using HIF-1$\alpha$ ASODN sequence to block endogenous HIF-1 production may be an operative approach for gene therapy in antitumor through cleaving the target mRNA or inhibiting mRNA transcription. The bare HIF-1$\alpha$ ASODN fragment, however, exists many defects when delivered *in vivo*, such as non-specific, earlier degradation, poor cellular internalization, and lysosomal trapping. In the present study, the novel HIF-1$\alpha$ ASODN-loaded nanocomposite was prepared and characterized as a gene delivery system. The introduction of gelatin core in GEL-DGL-FA-ASODN-DCA nanocomposite provided a desired size range of 170–192 nm for prolonging blood circulation time and enhancing permeability and retention effect. FA and DCA were conjugated to DGL in turn to improve the specificity to tumor and escape from lysosomes. *In vitro* cellular uptake behaviors and cytotoxicity assay indicated consistently the preferential aggregation capability of the resulting GEL-DGL-FA-ASODN-DCA nanocomposite to HepG2 and HeLa cells. The subcellular distribution images displayed clearly the lysosomal escape ability of vector. HIF-1$\alpha$ mRNA expression level analysis and HIF-1$\alpha$ protein assay testified that the GEL-DGL-FA-ASODN-DCA nanocomposite can synchronously inhibited mRNA expression and HIF-1$\alpha$ protein translation. *In vivo* optical images and quantitative assay verified that the GEL-DGL-FA-ASODN-DCA nanocomposite accumulated overwhelmingly in the tumor tissue. The high tumor inhibitory rate with 77.99% has powerfully proved the antitumor efficacy of GEL-DGL-FA-ASODN-DCA nanocomposite. In short, the resultant nanocomposite can enhance the specific targeting to tumor cells, reduce toxicity and side effects, and achieve escape from lysosomes. Finally, tumor growth was inhibited by the interaction of exogenous HIF-1$\alpha$ ASODN with the target RNA.

## Conflicts of interest

The authors report no conflicts of interest. The authors alone are responsible for the content and writing of this article.

## Acknowledgments

This study was supported by the National Natural Science Foundation of China Fund (No 81541060) and Science and Technology Projects from the Science Technology and Innovation Committee of Shenzhen Municipality (grant no. JCJY20170818110340383 and JCJY20170307163529489). The authors are grateful to Core Facility of School of Life Sciences, Lanzhou University for the assistance during some experiments.

## REFERENCES

[1] Siegel RL, Miller KD, Jemal A. Cancer statistics, 2018. CA Cancer J Clin 2018;68(1):7–30.
[2] Avila MA, Berasain C, Sangro B, Prieto J. New therapies for hepatocellular carcinoma. Oncogene 2006;25(27):3866–84.
[3] Morille M, Passirani C, Vonarbourg A, Clavreul A, Benoit JP. Progress in developing cationic vectors for non-viral systemic gene therapy against cancer. Biomaterials 2008;29(24–25):3477–96.
[4] Ardelt P, Böhle A. Molecular aspects of bladder cancer IV: gene therapy of bladder cancer. Eur Urol 2002;41(4):372–81.
[5] Le BT, Raguraman P, Kosbar TR, Fletcher S, Wilton SD, Veedu RN. Antisense oligonucleotides targeting angiogenic factors as potential cancer therapeutics. Mol Ther-Nucl Acids 2018;14:142–57.
[6] Mandl M, Kapeller B, Lieber R, Macfelda K. Hypoxia-inducible factor-1$\beta$ (HIF-1$\beta$) is upregulated in a HIF-1$\alpha$-dependent manner in 518A2 human melanoma cells under hypoxic conditions. Biochem Bioph Res Co 2013;434(1):166–72.
[7] Greenberger LM, Horak ID, Filpula D, Sapra P, Westergaard M, Frydenlund HF, et al. A rna antagonist of hypoxia-inducible factor-1$\alpha$, EZN-2968, inhibits tumor cell growth. Mol Cancer Ther 2008;7(11):3598–608.
[8] Gillespie DL, Whang K, Ragel BT, Flynn JR, Kelly DA, Jensen RL. Silencing of hypoxia inducible factor-1$\alpha$ by RNA interference attenuates human glioma cell growth *in vivo*. Clin Cancer Res 2007;13(8):2441–8.
[9] Xia Y, Choi HK, Lee K. Recent advances in hypoxia-inducible factor (HIF)-1 inhibitors. Eur J Med Chem 2012;49:24–40.
[10] Semenza GL. Hypoxia-inducible factor 1 (HIF-1) pathway. Sci Stke 2007;2007(407):cm8.
[11] Caniggia I, Mostachfi H, Winter J, Gassmann M, Lye SJ, Kuliszewski M, et al. Hypoxia-inducible factor-1 mediates the biological effects of oxygen on human trophoblast differentiation through TGF$\beta_3$. J Clin Invest 2000;105(5):577–87.
[12] Agrawal S, Iyer RP. Perspectives in antisense therapeutics. Pharmacol Therapeut 1997;76(1–3):151–60.
[13] Crooke ST. Molecular mechanisms of action of antisense drugs. Biochim Biophys Acta 1999;1489(1):31–43.
[14] Geary RS, Norris D, Yu R, Bennett CF. Pharmacokinetics, biodistribution and cell uptake of antisense oligonucleotides. Adv Drug Deliver Rev 2015;87:46–51.
[15] Lambert G, Fattal E, Couvreur P. Nanoparticulate systems for the delivery of antisense oligonucleotides. Adv Drug Deliver Rev 2001;47(1):99–112.
[16] Wagner RW. Gene inhibition using antisense oligodeoxynucleotides. Nature 1994;372(6504):333–5.
[17] Karaki S, Benizri S, Mejías R, Baylot V, Branger N, Nguyen T, et al. Lipid-oligonucleotide conjugates improve cellular uptake and efficiency of TCTP-antisense in castration-resistant prostate cancer. J Control Release 2017;258:1–9.
[18] Loke SL, Stein CA, Zhang XH, Mori K, Nakanishi M, Subasinghe C, et al. Characterization of oligonucleotide transport into living cells. P Natl Acad Sci USA 1989;86(10):3474–8.
[19] Yakubov LA, Deeva EA, Zarytova VF, Ivanova EM, Ryte AS, Yurchenko LV, et al. Mechanism of oligonucleotide uptake by cells: involvement of specific receptors? P Natl Acad Sci USA 1989;86(17):6454–8.
[20] Wong SY, Pelet JM, Putnam D. Polymer systems for gene delivery-past, present and future. Prog Polym Sci 2007;32(8–9):799–837.
[21] Huang R, Ke W, Han L, Li J, Liu S, Jiang C. Targeted delivery of chlorotoxin-modified DNA-loaded nanoparticles to glioma

via intravenous administration. Biomaterials 2011;32(9):2399–406.
[22] Yamashiro DJ, Fluss SR, Maxfield FR. Acidification of endocytic vesicles by an ATP-dependent proton pump. J Cell Biol 1983;97(3):929–34.
[23] Behr JP. The proton sponge: a trick to enter cells the viruses did not exploit. Chimia 1997;51(1–2):34–6.
[24] Mindell JA. Lysosomal acidification mechanisms. Annu Rev Physiol 2012;74:69–86.
[25] Lee JH, Lim YB, Choi JS, Kim TI, Kim HJ, Yoon JK, et al. Polyplexes assembled with internally quaternized PAMAM-OH dendrimer and plasmid DNA have a neutral surface and gene delivery potency. Bioconjugate Chem 2003;14(6):1214–21.
[26] Boussif O, Lezoualc' HF, Zanta MA, Mergny MD, Scherman D, Demeneix B, et al. A versatile vector for gene and oligonucleotide transfer into cells in culture and *in vivo*: polyethylenimine. P Natl Acad Sci U S A 1995;92(16):7297–301.
[27] Fischer D, Bieber T, Li Y, Elsässer HP, Kissel T. A novel non-viral vector for DNA delivery based on low molecular weight, branched polyethylenimine: effect of molecular weight on transfection efficiency and cytotoxicity. Pharm Res 1999;16(8):1273–9.
[28] Malik N, Wiwattanapatapee R, Klopsch R, Lorenz K, Frey H, Weener JW, et al. Dendrimers: relationship between structure and biocompatibility *in vitro*, and preliminary studies on the biodistribution of $^{125}$I-labelled polyamidoamine dendrimers *in vivo*. J Control Release 2000;65(1–2):133–48.
[29] Huang R, Liu S, Shao K, Han L, Ke W, Liu Y, et al. Evaluation and mechanism studies of PEGylated dendrigraft poly-L-lysines as novel gene delivery vectors. Nanotechnology 2010;21(26):265101–11.
[30] Cottet H, Martin M, Papillaud A, Souaïd E, Collet H, Commeyras A. Determination of dendrigraft poly-L-lysine diffusion coefficients by taylor dispersion analysis. Biomacromolecules 2007;8(10):3235–43.
[31] Tsogas I, Theodossiou T, Sideratou Z, Paleos CM, Collet H, Rossi JC, et al. Interaction and transport of poly(L-lysine) dendrigrafts through liposomal and cellular membranes: the role of generation and surface functionalization. Biomacromolecules 2007;8(10):3263–70.
[32] Tomalia DA, Fréchet JMJ. Discovery of dendrimers and dendritic polymers: a brief historical perspective. J Polym Sci A1 2002;40(16):2719–28.
[33] Kodama Y, Nakamura T, Kurosaki T, Egashira K, Mine T, Nakagawa H, et al. Biodegradable nanoparticles composed of dendrigraft poly-L-lysine for gene delivery. Eur J Pharm Biopharm 2014;87(3):472–9.
[34] Ohsaki M, Okuda T, Wada A, Hirayama T, Niidome T, Aoyagi H. *In vitro* gene transfection using dendritic poly(L-lysine). Bioconjugate Chem 2002;13(3):510–17.
[35] Hofman J, Buncek M, Haluza R, Streinz L, Ledvina M, Cigler P. *In vitro* transfection mediated by dendrigraft poly(L-lysines): the effect of structure and molecule size. Macromol Biosci 2013;13(2):167–76.
[36] Zhou C, Long M, Qin Y, Sun X, Zheng J. Luminescent gold nanoparticles with efficient renal clearance. Angew Chem Int Edit 2011;50(14):3168–72.
[37] Stylianopoulos T, Wong C, Bawendi MG, Jain RK, Fukumura D. Multistage nanoparticles for improved delivery into tumor tissue. Method Enzymol 2012;508:109–30.
[38] Thode K, Lück M, Schröder W, Wolfhard S, Blunk T, Müller RH, et al. The influence of the sample preparation on plasma protein adsorption patterns on polysaccharide-stabilized iron oxide particles and N-terminal microsequencing of unknown proteins. J Drug Target 1997;5(1):35–43.
[39] Sakurai F, Nishioka T, Yamashita F, Takakura Y, Hashida M. Effects of erythrocytes and serum proteins on lung accumulation of lipoplexes containing cholesterol or dope as a helper lipid in the single-pass rat lung perfusion system. Eur J Pharm Biopharm 2001;52(2):165–72.
[40] Cai X, Dong C, Dong H, Wang G, Pauletti GM, Pan X, et al. Effective gene delivery using stimulus-responsive catiomer designed with redox-sensitive disulfide and acid-labile imine linkers. Biomacromolecules 2012;13(4):1024–34.
[41] Mintzer MA, Simanek EE. Nonviral vectors for gene delivery. Chem Rev 2009;109(2):259–302.
[42] Hu G, Wang Y, He Q, Gao H. Multistage drug delivery system based on microenvironment-responsive dendrimer-gelatin nanoparticles for deep tumor penetration. RSC Adv 2015;5(104):85933–7.
[43] Perrault SD, Walkey C, Jennings T, Fischer HC, Chan WCW. Mediating tumor targeting efficiency of nanoparticles through design. Nano Lett 2009;9(5):1909–15.
[44] Lei D, Yang W, Gong Y, Jing J, Nie H, Yu B, et al. Non-covalent decoration of carbon dots with folic acid via a polymer-assisted strategy for fast and targeted cancer cell fluorescence imaging. Sensor Actuat B-Chem 2016;230:714–20.
[45] Liu M, Liu L, Wang X, Shuai W, Hu Y, Han M, et al. Folate receptor-targeted liposomes loaded with a diacid metabolite of norcantharidin enhance antitumor potency for H22 hepatocellular carcinoma both *in vitro* and *in vivo*. Int J Nanomed 2016;11:1395–412.
[46] Cotten M, Wagner E, Zatloukal K, Phillips S, Curiel DT, Birnstiel ML. High-efficiency receptor-mediated delivery of small and large (48 kilobase gene constructs using the endosome-disruption activity of defective or chemically inactivated adenovirus particles. P Natl Acad Sci USA 1992;89(13):6094–8.
[47] Russ V, Wagner E. Cell and tissue targeting of nucleic acids for cancer gene therapy. Pharm Res 2007;24(6):1047–57.
[48] Meyer M, Dohmen C, Philipp A, Kiener D, Maiwald G, Scheu C, et al. Synthesis and biological evaluation of a bioresponsive and endosomolytic siRNA-polymer conjugate. Mol Pharm 2009;6(3):752–62.
[49] Cho YW, Kim JD, Park K. Polycation gene delivery systems: escape from endosomes to cytosol. J Pharm Pharmacol 2003;55(6):721–34.
[50] Sanjoh M, Hiki S, Lee Y, Oba M, Miyata K, Ishii T, et al. pDNA/poly(L-lysine) polyplexes functionalized with a pH-sensitive charge-conversional poly(aspartamide) derivative for controlled gene delivery to human umbilical vein endothelial cells. Macromol Rapid Comm 2010;31(13):1181–6.
[51] Russell PJ, Hewish D, Carter T, Sterling-Levis K, Ow K, Hattarki M, et al. Cytotoxic properties of immunoconjugates containing melittin-like peptide 101 against prostate cancer: *in vitro* and *in vivo* studies. Cancer Immunol Immun 2004;53(5):411–21.
[52] Masago K, Itaka K, Nishiyama N, Chung UI, Kataoka K. Gene delivery with biocompatible cationic polymer: pharmacogenomic analysis on cell bioactivity. Biomaterials 2007;28(34):5169–75.
[53] Zhou Z, Shen Y, Tang J, Fan M, Kirk EAV, Murdoch WJ, et al. Charge-reversal drug conjugate for targeted cancer cell nuclear drug delivery. Adv Funct Mater 2009;19(22):3580–9.
[54] Yi H, Liu P, Sheng N, Gong P, Ma Y, Cai L. In situ crosslinked smart polypeptide nanoparticles for multistage responsive tumor-targeted drug delivery. Nanoscale 2016;8(11):5985–95.
[55] Yu L, Xie M, Li Z, Lin C, Zheng Z, Zhou L, et al. Facile construction of near-monodisperse and dual responsive polycarbonate mixed micelles with the ability of pH-induced

charge reversal for intracellular delivery of antitumor drugs. J Mater Chem B 2016;4(36):6081–93.
[56] Yu L, Tan S, Li Z, Zheng Z, Zhou L, Su Y, et al. Mixed polycarbonate prodrug nanoparticles with reduction/pH dual-responsive and charge conversional properties. React Funct Polym 2017;120:74–82.
[57] Coester CJ, Langer K, Von Briesen H, Kreuter J. Gelatin nanoparticles by two step desolvation a new preparation method, surface modifications and cell uptake. J Microencapsul 2000;17(2):187–93.
[58] Zhang J, Li S, An F, Liu J, Jin S, Zhang J, et al. Self-carried curcumin nanoparticles for *in vitro* and *in vivo* cancer therapy with real-time monitoring of drug release. Nanoscale 2015;7(32):13503–10.
[59] Tang M, Dong H, Li Y, Ren T. Harnessing the PEG-cleavable strategy to balance cytotoxicity, intracellular release and the therapeutic effect of dendrigraft poly-L-lysine for cancer gene therapy. J Mater Chem B 2016;4(7):1284–95.
[60] Mumcuoglu D, Sardan M, Tekinay T, Guler MO, Tekinay AB. Oligonucleotide delivery with cell surface binding and cell penetrating peptide amphiphile nanospheres. Mol Pharm 2015;12(5):1584–91.
[61] Varkouhi AK, Scholte M, Storm G, Haisma HJ. Endosomal escape pathways for delivery of biologicals. J Control Release 2011;151(3):220–8.
[62] Albanese A, Tang PS, Chan WCW. The effect of nanoparticle size, shape, and surface chemistry on biological systems. Annu Rev Biomed Eng 2012;14:1–16.
[63] Juliano RL. The delivery of therapeutic oligonucleotides. Nucleic Acids Res 2016;44(14):6518–48.
[64] Gosselin MA, Guo WJ, Lee RJ. Efficient gene transfer using reversibly cross-linked low molecular weight polyethylenimine. Bioconjugate Chem 2001;12(6):989–94.
[65] Chirila TV, Rakoczy PE, Garrett KL, Lou X, Constable IJ. The use of synthetic polymers for delivery of therapeutic antisense oligodeoxynucleotides. Biomaterials 2002;23(2):321–42.
[66] Akbarzadeh F, Khoshgard K, Arkan E, Hosseinzadeh L, Azandaryani AH. Evaluating the photodynamic therapy efficacy using 5-aminolevulinic acid and folic acid-conjugated bismuth oxide nanoparticles on human nasopharyngeal carcinoma cell line. Artif Cell Blood Sub 2018;46(sup3):S514–23.
[67] Chen K, Chen Q, Wang K, Zhu J, Li W, Li W, et al. Synthesis and characterization of a PAMAM-OH derivative containing an acid-labile $\beta$-thiopropionate bond for gene delivery. Int J Pharm 2016;509(1–2):314–27.
[68] Wang C, Cheng L, Liu Z. Drug delivery with upconversion nanoparticles for multi-functional targeted cancer cell imaging and therapy. Biomaterials 2011;32(4):1110–20.
[69] Crooke ST. Progress toward oligonucleotide therapeutics: pharmacodynamic properties. FASEB J 1993;7(6):533–9.
[70] Bennett CF, Swayze EE. RNA targeting therapeutics: molecular mechanisms of antisense oligonucleotides as a therapeutic platform. Annu Rev Pharmacol 2010;50:259–93.
[71] Shen L, Zhao X, Zhou S, Lu Z, Zhao K, Fan J, et al. *In vivo* evaluation of the effects of simultaneous inhibition of GLUT-1 and HIF-1$\alpha$ by antisense oligodeoxynucleotides on the radiosensitivity of laryngeal carcinoma using micro 18F-FDG pet/ct. Oncotarget 2017;8(21):34709–26.
[72] Kobayashi H, Watanabe R, Choyke PL. Improving conventional enhanced permeability and retention (EPR) effects; what is the appropriate target? Theranostics 2014;4(1):81–9.
[73] Liu X, Chen Y, Li H, Huang N, Jin Q, Ren K, et al. Enhanced retention and cellular uptake of nanoparticles in tumors by controlling their aggregation behavior. ACS Nano 2013;7(7):6244–57.